Chapter 1

INTRODUCTION AND LITERATURE REVIEW

This chapter gives an overview of photodetection theory, the discussion of conventional photodetection structures and their limitation for efficient broadband applications. This chapter further investigates the requisites for broadband photodetection with an extensive literature review and had explored new low dimensional materials and studied their simple and hybrid photodetection structures. Out of various low dimensional materials, two-dimensional (2D) materials like graphene, SnS_2 and zero-dimensional (0D) nanostructure like Cu_2SnS_3 and their combination (0D/2D) with other low dimensional materials have been explored due to their favourable optoelectronic properties for broadband photodetection. In the later half section of this chapter an extensive literature review on 0D, 2D and their hybrid (0D/2D) structures for broadband photodetection have been done. Some preliminary work on the CTS nano structures/ QDs, 2D-graphene and layered TMDs based broadband photodetection have been explored in terms of their optical characteristics, synthesis techniques, fabrication complexity etc. Finally the hybrid structures of 2D-graphene and 2D-SnS_2 with others OD-QDs structures has been investigated to explore the research gap

1.1 Introduction

Photodetectors are the pivotal optoelectronic components in miniaturized electronic industry that translate the optical signals into electrical signals and therefore, have received extensive attention in various fields. There are generally three steps involved in photodetection process named as detection of photon energy, generation of photocarriers and then the collection of photocarriers. In the realization of efficient photodetection for a band of light, the selection of appropriate active materials demands extensive investigation for next-generation applications. The active materials in photodetectors structures should hold the potentiality to absorb the photon energy more or equal to their electronic band gap and should result in photogenerated carriers. These generated carriers are then transported to the electrodes before recombination within the materials, and manifested as the photocurrent. Photodetection in various sub-bands are having their potentiality in a large range of applications like video imaging, optical communications, biomedical imaging, security, night-vision, and motion detection [13, 14, 15]. The evaluation of the performance of any photodetector is performed in terms of various factors like good sensitivity for the optical wavelengths, efficient photon to electron conversion, fast responsive to the optical signal, low noise, high reliability and low cost.

1.2 Photodetection Theory

Photodetection process generally consists of three processes which includes the absorption of the optical signal, generation of photo-carriers and finally the transportation and collection of these photo-charge carriers.

1.2.1 Absorption

The absorption of light is the basic and initial photodetection process involved in the photodetection structure. On the basis of absorption in the active materials, photodetectors are classified as intrinsic and extrinsic type [16] as illustrated in Fig.1.1. When

a semiconductor is illuminated with the photons energy greater or equal to the band gap (E_g) of semiconductor material, the excitation of electrons takes place from the valence band (VB) to the conduction band (CB) and it is called intrinsic photodetection as shown in Fig.1.1 (a). Whereas, if the material is illuminated with the photon energy less than the band gap of material there is still a transition of charge carriers which takes place from deep impurity and defect levels within the band gap named as extrinsic transitions, shown in Fig.1.1 (b). There is one important type of extrinsic photodetectors which has been realized by the quantum well structure as shown in Fig.1.1 (c). The small sub band energy transitions (energy <100 meV) make these kinds of detectors suitable for small energy detection applications for far infrared (FIR) range optical signals. [16].

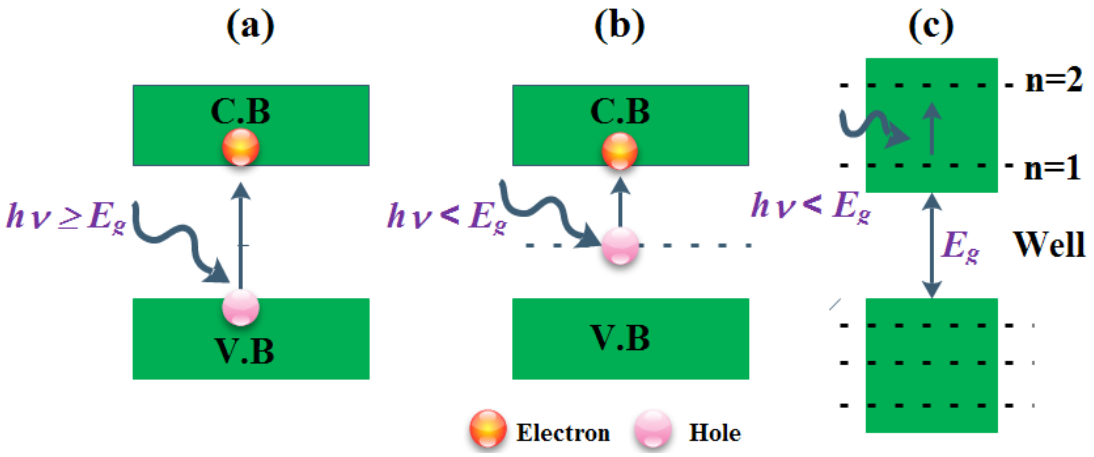

Figure 1.1: Carriers transition under light illumination (a) Intrinsic transition ($h\upsilon \geq E_g$), (b) Extrinsic transition ($h\upsilon < E_g$) from trap energy state (c) Extrinsic transition in quantum well structure

The absorption of light in a semiconductor is indicated by the absorption coefficient (α) of the materials. The absorption coefficient of the material is an important parameter which not only determines the capability of photon absorption but also gives the information where the light will be absorbed. Most of the photon absorption (about 63%) occurs over a distance $1/\alpha$. It is called penetration depth of absorber materials [1]. A high value of absorption coefficient indicates the absorption of light at the surface of the semiconductor materials while the smaller value of the absorption coef-

ficient results in the deep penetrations in the semiconductor materials without giving appreciable photo-excitation [1]. The intrinsic absorption coefficients for various photodetector materials used for broadband photodetection are shown in Fig.1.2, where the solid line denotes the absorption coefficient for 300 K while dashed curves are for 77K [1]. So in brief, since α is a strong function of wavelength, for a given semiconductor the wavelength range in which appreciable photocurrent can be generated is limited.

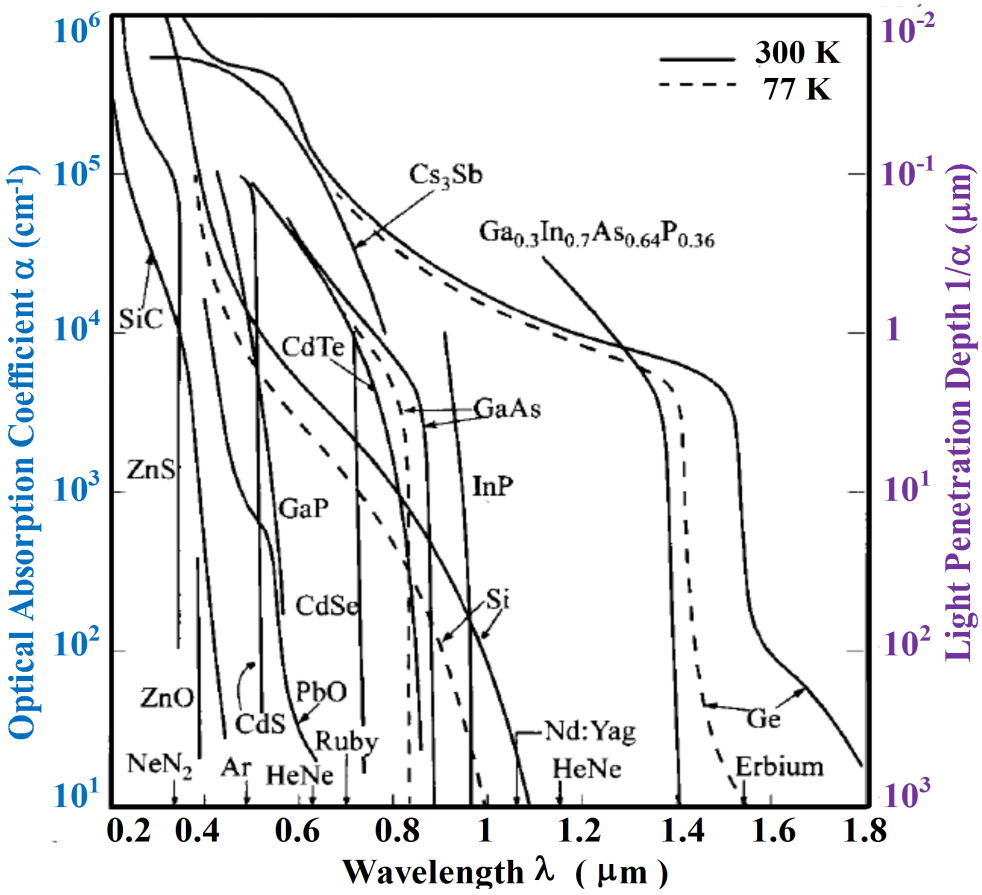

Figure 1.2: Optical absorption co-efficient of some UV-Vis-NIR photodetector materials with light penetration depth (From Ref. [1])

1.2.2 Photocurrent Generation Mechanisms

There are mainly three mechanisms that have been involved in the generation of the photocarriers manifested as a photocurrent, classified as photoconductive, photovoltaic, and thermoelectric. In first two mechanisms that is photoconductive and photovoltaic,

the photon energy is used to excite the carriers which are responsible to contribute the photocurrent. This type of detectors are widely used in broad range (UV-Vis-NIR) of applications including optical communication and solar cell. While in thermoelectric mechanism, the detectors detect the light by sensing the temperature rise when light energy is absorbed at their dark surface. These detectors are having their applications in far-infrared direction like thermal imaging, remote sensing, etc. [17, 18]

1.2.2.1 Photoconductive Effects

The generation of photocarriers by incident photon energy which increases the conductance of semiconductor materials is called the photoconductive effect as shown in Fig.1.3. The current flow in the structure without any illumination is called dark current (I_{dark}) which exists in the structure due to the small thermal energy of carriers collected by external biasing. When the device is illuminated with photon energy greater and equal to the band gap of material as shown in Fig.1.3 (b), the generation of electron hole pairs takes place. The generated electron-hole pairs are then transferred to the opposite electrode by the applied voltage (V) and result in a photocurrent (I_{photo}) which result in the increase in the photo-conductivity of the photodetector [19, 20, 21].

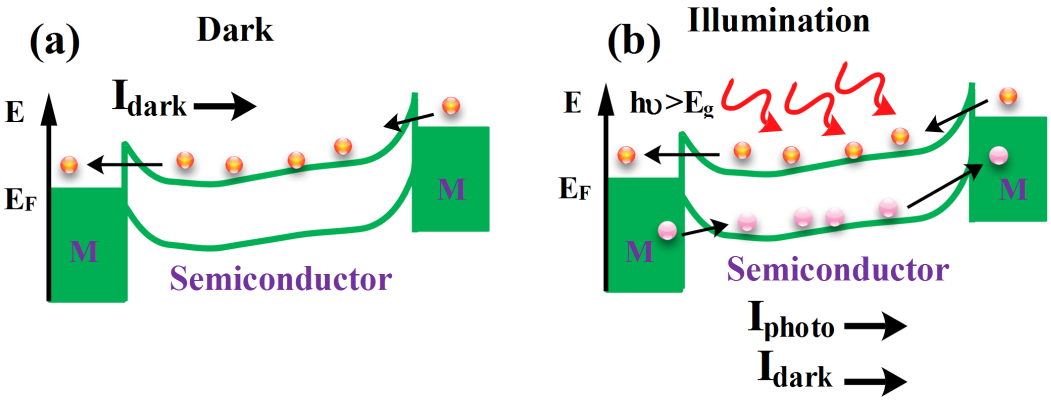

Figure 1.3: Photoconductive mechanism (a) Under dark and, (b) Illumination condition

1.2.2.2 Photovoltaic Effects

In the photo voltaic mechanism the photogenerated carriers in the semiconductor are separated by an internal electric field. Some interfaces can build the internal electric field, such as the Schottky barrier or a PN junction. Under these circumstances, the detectors exhibit nonlinear I–V properties in the dark. When such devices are illuminated with zero external bias the internal electric field separates the photo excited carriers (electron and hole) and generate a current called short circuit current in photovoltaic device nomenclature. The accumulation of carriers of opposite polarity develops an open circuit voltage across the detector denoted by V_{OC} [22]. Under light illumination with reverse bias, the photogenerated carriers are wiped out in opposite directions, leading to the increasing magnitude of the reverse current. The lowest dark current in the photovoltaic effect-based structures under no bias condition make them efficient detectors in terms of detectivity. But, the photo responsivity is smaller than the devices which works at the photo conducting mechanism because of the deficiency of the internal gain.

1.2.2.3 Photo-thermoelectric Effects

In photo-thermoelectric effects (PTE) the change in a temperature gradient in the semiconductor channel has been observed by impinging the appropriate wavelength on the detection structure. Due to temperature gradient a temperature difference (ΔT) between the two ends of the semiconductor channel is observed . The temperature difference between the channel is then converted into voltage different (ΔV) via the Seebeck effect. The magnitude of (ΔV) is linearly proportional to the temperature gradient via the Seebeck coefficient (S) and formulated as $\Delta V = S.\Delta T$ [22].

1.2.3 Figure of Merits (FOMs) of Photodetectors

Figure of merits (FOMs) of a photodetector is defined by the optical parameters which tells the performance of any photodetection structure. These performance indices of any photodetector can be evaluated from the current-voltage (I-V) characteristics under

dark and illuminated conditions. Apart from I-V characteristics other performance parameters such as quantum efficiency, responsivity, sensitivity, detectivity and time response are the major FOMs of any photodetection structure.

1.2.3.1 Sensitivity (S)

The sensitivity of the photodetector is defined as the ratio of photon current to the dark current for a given applied bias. It is also called the contrast ratio in some optical nomenclature [23]. The sensitivity of the detector for an incident optical power is given by

$$Sensitivity\ (S) = \frac{I_{photon}}{I_{dark}} \tag{1.1}$$

where, I_{photo}=I_{light}-I_{dark} is photon current and I_{Dark} is dark current.

1.2.3.2 External Quantum Efficiency (EQE)

The external quantum efficiency of the photodetector is defined as the number of electron-hole pairs (EHPs) collected to the number of photons of given energy incident on the detector. The external quantum efficiency is denoted by η and defined as

$$EQE\ (\eta) = \frac{Number\ of\ EHPs\ Generated\ and\ Collected}{Number\ of\ Incident\ Photons} = \frac{I_{photon}/e}{P_{opt}/h\upsilon} \tag{1.2}$$

where, P_{opt} is illuminated power, e is electronic charge, h is Plank's constant, and υ is the frequency.

1.2.3.3 Responsivity (A/W)

Responsivity of the detectors is defined as the generated outcome (current or voltage) per incident optical power at an incident wavelength (λ) and expressed in A/W or V/W [24, 25]. The responsivity of the photodetector in term of (A/W) is defined as

$$Responsivity\ (A/W) = \frac{Photocurrent\ (A)}{Incident\ Optical\ Power\ (W)} = \frac{I_{photon}}{P_{opt}} \tag{1.3}$$

where, P_{opt} is illuminated power and I_{photon} is the photon current

1.2.3.4 Specific Detectivity (cm.Hz$^{1/2}$.W^{-1} or Jones)

The detectivity of the photodetection structures defined the ability to measure the minimum detectable signal. The detectivity of any photodetection structure is denoted by the inverse of noise equivalent power (NEP). The NEP of the photodetector is defined as the minimum required optical power to illuminate the detector to produce the signal to noise ratio (S/N) unity in 1-Hz of bandwidth. The detectivity of a detector is given by D=(NEP)$^{-1}$. The specific (or normalized) detectivity (D*) of the detector related to the NEP is defined as [24, 25]

$$Detectivity\ (D^*) = \frac{\sqrt{AB}}{NEP} = \frac{\sqrt{AB}}{i_{noise}/R} \tag{1.4}$$

where, A is the effective area of photodetectors, B is the electrical bandwidth, i_{noise} is the noise current and R is the responsivity of photodetectors. When the dark current is dominated by the shot noise, D* can be expressed as [12, 26]

$$Detectivity\ (D^*) = \frac{R}{\sqrt{2qJ_{dark}}} \tag{1.5}$$

where, J_{dark} is the dark current density for an applied bias of photodetectors and q is electronic charge.

1.2.3.5 Time Response

The time response of the photodetector is expressed in terms of the rise time (t_r) and fall time (t_f) of the output signal when a pulsed light is incident on the detector[12]. The rise time is the measure of the time response of a photo diode to a stepped light input and is defined as the time required for the output to change from 10% to 90% of the steady output level. Similarly, the fall time is measured as the decay from the 90% to 10% of the falling edge of the output rectangular pulses of the detector when a

pulsed source of light is incident on the detector.

1.3 Typical Photodetector Structures

The photodetector structures are broadly classified into three categories (1) Photodiode structure (2) Phototransistor and (3) photoconductor. The diode type photodetection structures are further classified as p-n photodiode, pin photodiode, avalanche photodiode and Schottky photodiode.

1.3.1 Photodiode

A photodiode is a junction diode operated with an reverse-biased voltage. A pn photodiode is the most common photodetection device used in a multitude of ordinary and specialized applications. When the photodiode structures are illuminated by appropriate photon energy the electron hole pairs are generated. The generated photocarriers then swept out and transported to the electrodes due to the electric field in the depletion region [1]. The transported photo carries are then collected at the electrode and result in a photocurrent.

1. **pn-Photodiode** – A pn diode is the basic type of photodiode structure works under reverse bias condition to generate an electron hole pairs. The generated electron hole pairs under the influence of incident light are transported to the electrode by the existing electric field and result in photocurrent. A reverse bias pn junction when used to detect light is shown in Fig.1.4 (a). The incident photons create extra electron hole pairs in the semiconductor which are known as photogenerated carriers. The photocarriers in the depletion region are drifted instantaneously under the influence of electric field across the junction and hence contribute in photocurrent. Whereas, the electron hole pairs generated outside the depletion region(in neutral region) have to diffuse up to the junction boundary to be swept by the electric field. If the carriers are generated faraway (more than diffusion length) then the probability of its contribution in photocurrent is negligible. Therefore, the carriers generated in depletion width are primarily responsible for resultant photocurrent. For short depletion width the efficiency of the pn diode will

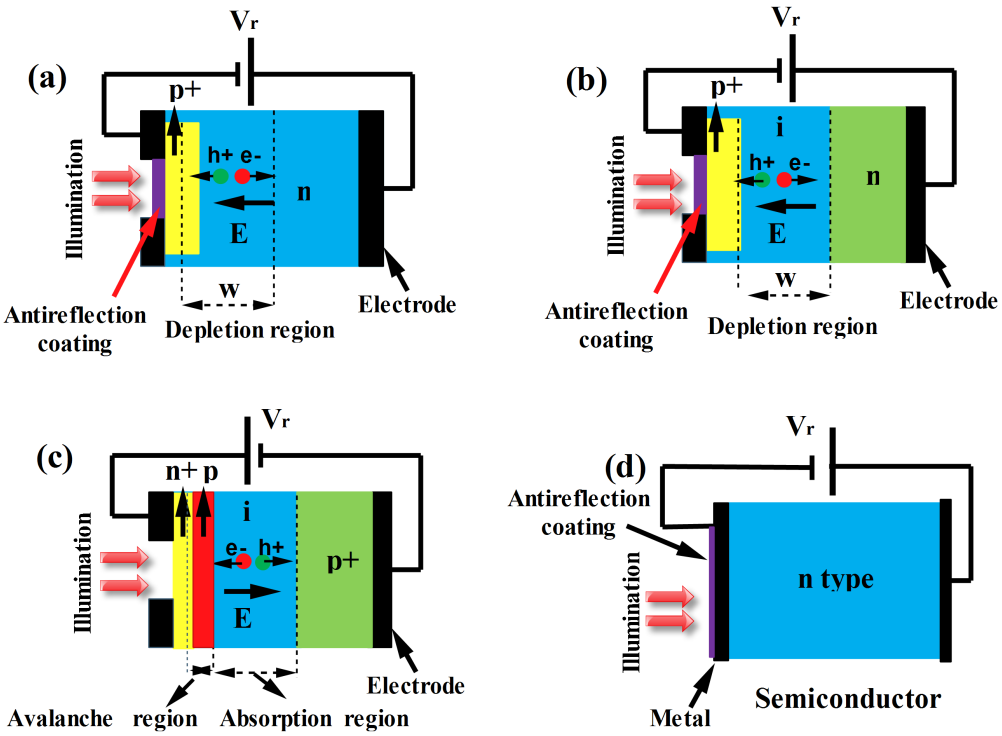

Figure 1.4: Schematic of a (a) pn, (b) pin, (c) Avalanche, and (d) Schottky type photodiode structures

be small. The diffusion is inherently is a slow process hence the performance of pn-photodiode is limited by the extra carrier generated outside the depletion regions. The limitation of small depletion layer width in pn photodiode have been further improved by sandwiching a intrinsic layer between p and n regions and results a pin photodiode [27].

2. **pin-Photodiode** – The pin photodiode is a junction diode in which an undoped i-region is inserted between p and n regions as shown in Fig.1.4 (b). Due to the low density of free carriers in undoped i-region and its high resistivity, any applied bias in this type of structures drop almost entirely across the i-region. In the results, the i-region in pin structure offers large depletion width throughout the intrinsic layer between the n and p doped semiconductor unlike the pn photodiode. Therefore, pin structure offers high responsivity, EQE in comparison to pn structure but have unity gain. The gain in the photodetection structure is defined as the ratio of the recombination time of photo carriers to transit time of photo carriers [1]. Although, pin structures are unity gain

structures but they offer large bandwidth. The speed of pin diodes is invariably limited by the transit time of photogenerated carriers [1].

3. **Avalanche Photodiode** – The avalanche Photo diodes are the photodetection structures that are used to sense small photon flux and convert them into large photocurrent through multiplication process resulting from impact ionization [27]. Avalanche photodetectors are more demanding in the detection of low level of light energy. Fig.1.4 (c) shows a typical avalanche photodiode structure with absorption and avalanche or gain region. A photodiode structure is operated at reverse biased with the reverse voltage close to breakdown voltage. Photo-generated carriers in the absorption or depletion region will travel at their saturation velocities, and will acquire sufficient energy which will result ionized collision with the lattice [27]. The ionized collision with lattice will produce the secondary electron-hole pairs which are drifted toward the electrodes with the primary photocarriers and results in the carriers multiplication and gain. In the results, avalanche photodiode offers large gain ($\sim$ 200 or more) but are noisy due to the random generation of photo carriers. They also offer complex design techniques.

4. **Schottky Photodiode** –Schottky photodiode is a structure which is formed by the a metal and a semiconductor material as depicted in Fig.1.4 (d). Depending upon the properties of the semiconductor and metal, a barrier is formed at the interface of metal and semiconductor material. This barrier results into bending of the bands. With the application of voltage, the bands can be bended more or less [1, 28]. In this region of band bending, electron hole pairs can easily be separated and results in photocurrent. The metal-semiconductor junction results a fast switching photodiode where the photocurrent depends on the majority carriers. Although Schottky diodes have small turn on voltage due to the fast recovery time of carriers, they do have some disadvantages or limitations. The reflection and absorption of light in the metal layers at longer wavelengths degrade their performance over pin structure [29]. To prevent the light reflection, an anti reflection coating is often applied, but this complicates the manufacture of such devices. The limitation of fabrication complexity of schottky photodiode prevents their use in high speed applications where the accuracy of the detection will be the primary objective [29].

1.3.2 Phototransistor

The photo transistor uses the transistor gain action in conjunction with the carrier generation due to light absorption. The transistor has a large base area (lightly doped) to collect the photons, at the base and collector depletion region. This is unlike a conventional bipolar junction transistor (BJT), where the base is usually thin to prevent carrier loss due to recombination (when the carriers move from emitter to collector). This accumulation of carriers at the base lowers the potential and increases the efficiency of the transfer of carriers from the emitter to the collector. Instead of a regular transistor, a hetero-junction transistor can also be used. Although offering good photo response photo-transistors suffers from the insensitive to incident light from other directions than particular narrow window unlike photo-resistor or photoconductor. Photo transistors are also susceptible to electricity surges in comparison to other photodetection structures [30].

1.3.3 Photoconductor

Photoconductors types of detection structures are the simplest detection structure among all other detection structures discussed above. This thesis is about to investigate single and hybrid semiconductor-based photoconductor structures to facilitate simplest and low-cost fabrication among other photodetection structures. Photoconductors are the photodetection structures where an active semiconductor absorber material is sandwiched between two metal electrodes as shown in Fig.1.5. Fig.1.5 (a) shows a typical photoconductor structure with a absorber active materials placed between two metal contacts. The channel length of the mentioned photoconductor structure is denoted by L while A is used to define the effective illumination area (A). There are typically two type of photoconductor structure named as lateral type and vertical type as shown in Fig.1.5 (b) and (c), respectively. The both device structures consists of two ohmic contacts placed on a semiconductor bar named as absorber [27]. The photodetection in the both photoconductor structure is governed by a photoconduction mechanism where the incident light changes the conductivity of the semiconductor materials and the change

in current is related by the conductivity of the semiconductor material. Among these two photoconductor structure lateral type structure offers easy fabrication process and also offers sufficient absorber area for photon interaction in comparison to the vertical type photoconductor structure [12].

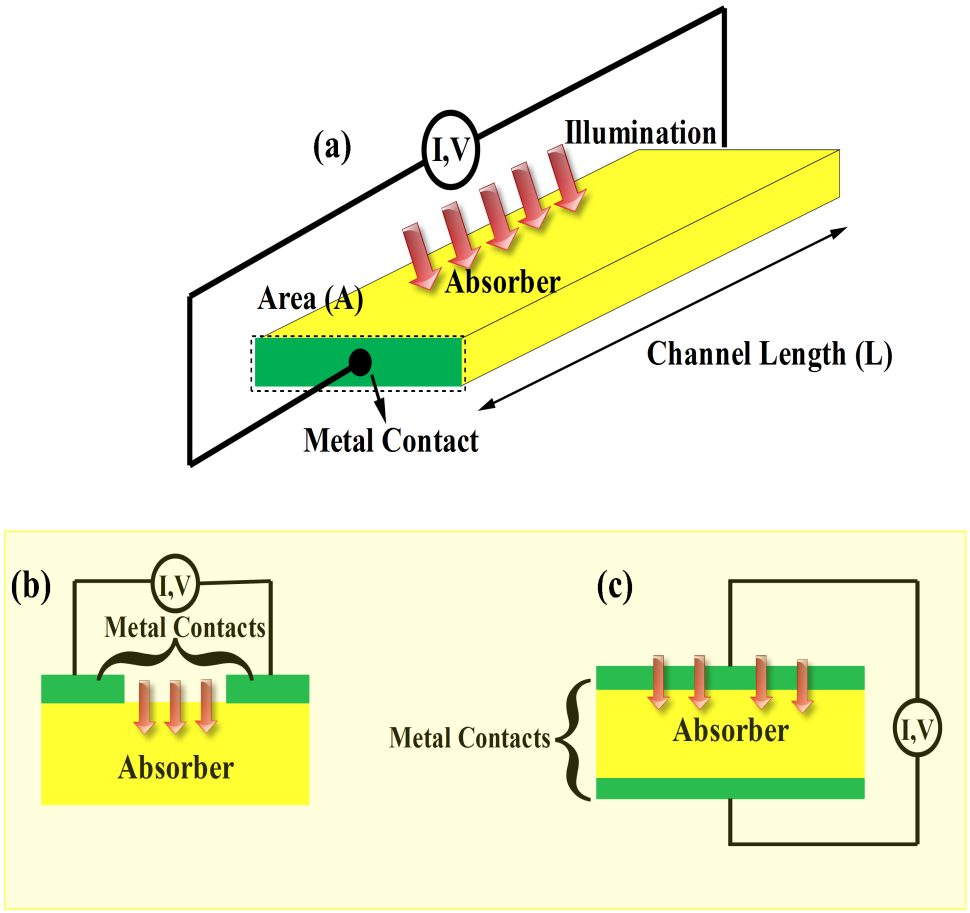

Figure 1.5: (a) A typical photoconductor structure with channel length (L) and effective illumination area (A): (b) Lateral type photoconductor (c) Vertical type photoconductor

When a photoconductor structures are illuminated by a appropriate photon energy the electron hole pairs are generated in semiconductor materials. The generated electron hole pairs reduce the conductivity of the active semiconductor material. As a result, the current flowing through the semiconductor bar increases with incident photon flux density for any fixed bias voltage applied between the two-metal electrode as shown in Fig.1.5. The change in current density (J) due to the incidence of photon can be represented as follow: The total current density, J in the semiconductor can be described

as

$$J = J_{dark} + J_{photo} \tag{1.6}$$

Where, J_{photo} is the photocurrent due to photogenerated carries and J_{dark} is the dark current in the device when no illumination take place. Let assuming the absorber semiconductor as n type in nature the current density of the semiconductor material in terms of conductivity (σ) and applied electric field (E) is given by

$$J = \sigma E \tag{1.7}$$

$$\sigma = \rho \mu_e \tag{1.8}$$

where, μ_e is the mobility of electrons and ρ is the charge density defined as

$$\rho = ne \tag{1.9}$$

where n is carrier concentration and e is the electronic charge.

The incident photon flux density (ϕ), increases equal electron (Δ n) and hole (Δ p) concentrations (i.e., Δ n= Δ p) due to photo-excited carriers. Thus, the photo current density due to incident photon flux can be defined as [31]

$$J_{photo} = (\mu_e + \mu_h)\Delta n e E \tag{1.10}$$

where μ_e and μ_h are electron and hole mobility respectively.

$$\Delta n = \frac{\eta \phi \tau}{LA} \tag{1.11}$$

where, η is quantum efficiency, τ is excess carrier recombination time, L is channel length of photoconductor, and A is the effective area of photoconductor as shown in Fig.1.5 (a).

Assuming v_e=$\mu_e E$, v_h=$\mu_h E$, t_e=L/v_e, and t_h=L/v_h as the drift velocity of electron,

drift velocity of hole, transit time of electron and transit time of hole, respectively. Now the photocurrent can be written as

$$i_{photo} = J_{photo}A = \eta\phi\tau e\left(\frac{1}{t_e} + \frac{1}{t_h}\right) \tag{1.12}$$

The photon flux density in term of incident optical power (P_{opt}) and λ of the photodetectors is defined as

$$\phi = \frac{P_{opt}}{h\upsilon} = \frac{P_{opt}\lambda}{hc} \tag{1.13}$$

From (1.12) and (1.13), the photoresponsivity of the detector is defined as [32]

$$R = \frac{I_{photo}}{P_{opt}} = \frac{\eta}{1240}\left(\frac{\tau}{t}\right)\lambda(nm) \tag{1.14}$$

where, $t = \left(\frac{1}{t_e} + \frac{1}{t_h}\right)^{1/2}$

Here, the factor τ/t defines the gain of the photoconductor and η is the quantum efficiency (i.e., number of carriers generated per photon). The value of τ and t depends on the type of materials used for the fabrication of the photoconductor and the channel length (L) of the fabricated detector.

Photoconductor type of structure offers high gain among all photo diode structures but their speed of operation is limited by the transit time of photo charge carriers. It has also offered the simplest design technique and having a wide range of applications due to its low-cost design [12].

1.3.3.1 Merits of Photoconductor Structures

The performance analysis of the various device structures are summarized in Table-1.1 and 1.2. The Table-1.1 [1] shows the sufficient gain in photoconductor structures while the speed of these detectors are limited by the transit time of charge carriers.

The comparison of photodetector parameters of different type of photo-conductors (lateral and vertical type) is given in Table-1.2 [12]. In this table the performance of the various structures are denoted by *, the more number of stars specifies the better

Table 1.1: Typical Values of Gain and Response Time for Photoconductor Structure over Some Common Photodetectors (From Ref. [1])

Photodetector		Gain	Response Time (s)
Photoconductor		$1\text{-}10^6$	$10^{-8}\text{-}10^{-3}$
Photodiode	p-n junction p-i-n junction metal semiconductor	1 1 1	10^{-11} $10^{-10}\text{-}10^{-8}$ 10^{-11}
Avalanche photodiode		$10^2\text{-}10^4$	10^{-10}
Phototransistor		10^2	10^{-6}

Table 1.2: Optical Performance of Lateral type Photoconductor over Other Photodetection Structures (From Ref. [12])

Performance Parameters	Photodiode	Photoconductor (vertical)	Photoconductor (lateral)	Phototransistor
Dark Current	*	****	***	***
On/off ratio	***	***	*****	*****
Responsivity	*	*****	****	*****
EQE	*	*****	****	*****
Gain	*	*****	****	*****
Response Time	*	***	*****	***
Complexity	***	*****	*	***

performance parameters for the various structures. The lateral type photoconductor has superiority in terms of its fabrication complexity. Apart from this it has the best on/off ratio in comparison to all other structures. In addition, they offer good responsivity, detectivity and EQE. The above properties of photoconductor structure motivated us to realize a broadband photodetection structure for broadband applications.

1.4 Broadband Photodetectors

Broadband photodetectors are photodetection structures that are used to detect the broad spectrum of light wavelengths by using a single detection structure. The broadband photodetection in these structures has been facilitated by integrating different

active materials into a single structure.

1.4.1 Applications of Broadband Photodetectors

The optical detectors have a fancy of applications in today's era due to their capability of detecting a bunch of wavelengths or a single wavelength. The optical spectrum window for photodetection is shown in Fig.1.6. The broadband photodetectors generally detect more than a band of the spectrum such as UV-Vis, Vis-NIR etc. The semiconductor material having a bandgap corresponding to the wavelength to be detected (as defined by $E_g = 1240/\lambda(nm)$), will be the appropriate choice for photodetection.

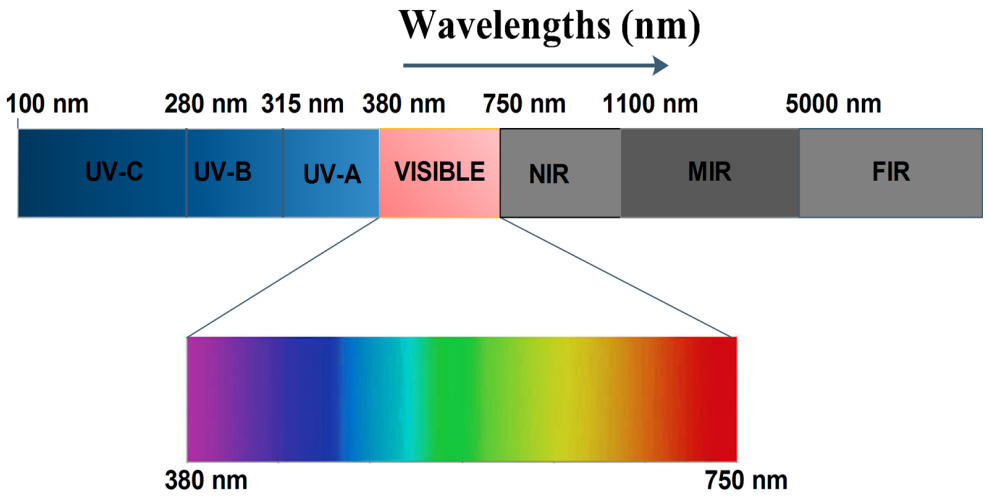

Figure 1.6: Electromagnetic spectrum of UV-Visible-Infrared as a function of wavelengths

Therefore, broadband photodetectors are the pivotal components in the modern optoelectronic industry. The detection of light in various sub bands have various applications which are discussed below separately.

UV-detection: UV radiation has a great impact on the survival and development of humankind for example, moderate skin exposure to natural or artificial UV light is advantageous for health, for instance, facilitating the synthesis of vitamin-D, killing germs, treating or preventing rickets, etc.[33, 34] Apart from these UV light detection has been used for environmental monitoring, military reconnaissance, space science, territory intrusions, sterilization, etc.

Visible Detection: The visible detector has been widely used for display, industrial safety, E-eyes, fingerprint printing, video imaging and industrial safety [26]. The visible band detector also have strong impact in the field of optical mapping from far distancing where the reach of mankind is not possible.

IR Detection: Infrared detector is more challenging due to very small amount of energies involved, comparable to the room temperature energy of the carriers which results in false detection. The infrared detector is generally made by narrow band semiconductor or by a quantum well structures where the transition of photocarriers take place between the sub band. Out of other spectrum bands like UV and visible these detectors have wide applications due to their capability of detecting small energy. Infrared (IR) light detection has been used for optical communications, night vision, remote control, analytical science, satellite remote sensing, fire alarming, precision strike, navigational aids, etc. [26]

Covering all the applications from UV to NIR are more challenging and demanding in today optoelectronic industry. A single device structure has been explored to detect the different band optical energy which not only decrease the production cost but also reduce the overall detection volume.

1.4.2 Traditional Materials for Broadband Photodetection

The traditional materials used for broadband photodetection are Si, Ge, InGaAs, HgCdTe, etc., have a wide range of applications in optoelectronics [26]. However, in traditional schemes, various photosensitive materials exploited have limited bandwidth, e.g., GaN [35] for UV (<400 nm), Si for Vis–near-IR (NIR, 400–1100 nm), Ge/InGaAs for NIR–mid-IR (MIR, 1–5 μm), and HgCdTe for MIR–far-IR (FIR, >5 μm) [26]. Fig.1.7 shows the optical responsivity of some traditional materials [36] used for broadband photodetection application covering UV, visible and NIR spectrum.

GaN/GaP materials have been used for UV/UV-Vis band photo-detection due to large band gap while Silicon is used as a strong visible-NIR material due to its moderate band gap about ∼1.1 eV [36]. The Si based photodetector shows the strong responsivity around at 970 nm which degrades in both directions i.e., toward UV and NIR

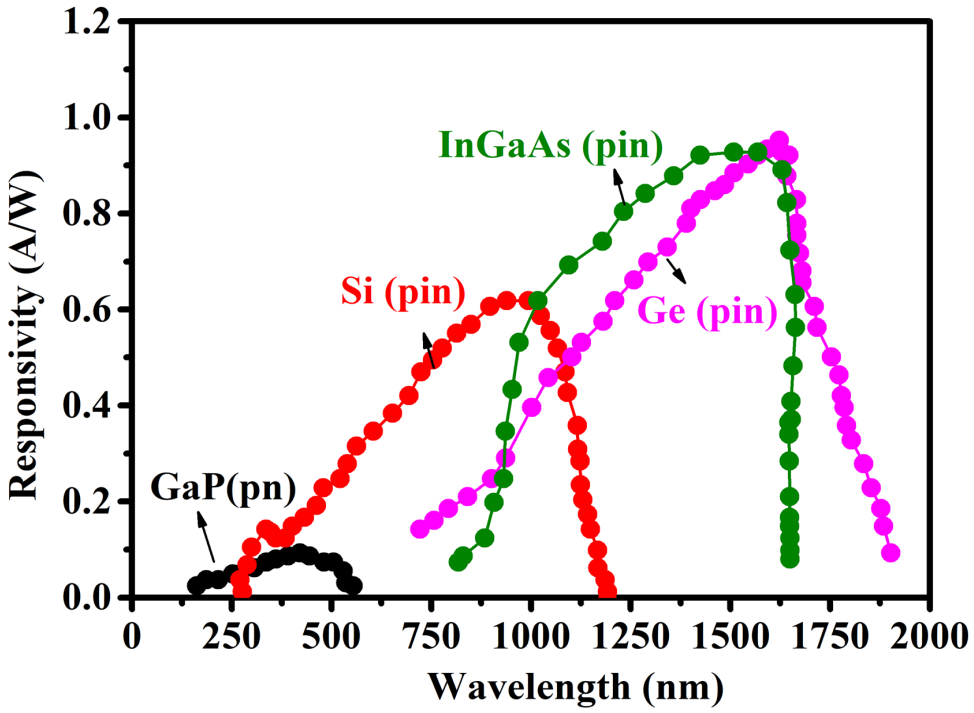

Figure 1.7: Photo responsivity of traditional materials used for UV-Visible-IR photodetection applications

regions as shown in Fig.1.7. The degradation in the optical performance of this material results either due to insufficient photon energy (NIR-side) or photon absorption at the surface due to presence of dangling bond (UV-side), therefore limit its performance as broadband photodetector [1]. The other materials like Ge, InGaAs based broadband photodetectors are having improved responsivity which results from good mobility of carriers in these materials in comparison to Si based structure and also having the capability of broadband detection in NIR regions. Advance fabrication techniques such as molecular beam epitaxy are required for these kind of materials which ultimately make the broadband photodetection costly [36].

Temperature dependent variation in the dark current of the traditional materials changes the performance of these detectors over broadband ranges and need a special kind of setup to maintain the suitable temperature for the optimized value of detectivity. For example, the detectivity of the prominent broadband photodetector based on HgCdTe shows the best detectivity of the order of 10^{10} Jones below room temperature i.e 77 K [37]. The performance of such detectors required a special cooling setup to

maintain desired temperature to optimize the performance in photodetection applications. The additional setup in these structures not only enhances the overall fabrication cost but also increase the overall detection volume in these devices. The detectivity is the characteristic of the photodetector that is related to the noise performance. The higher the detectivity the better is the performance of the device in a noisy environments. The calculated detectivity of various broadband traditional materials has been discussed by J.W. Zeller *et al.,* [37].

1.4.3 Limitations and Challenges of Traditional Materials in Broadband Photodetection

The poor optical parameters like, limited responsivity (as shown in Fig.1.7) [36] and low detectivity [37] of Silicon-based detectors limit its application in broadband photodetection. The fixed band gap nature of such materials hamper their optoelectronic properties for a broad range of applications including optical communication and night vision. Apart from Si other materials like InGaAs, InP, HgCdTe, etc., have been integrated to realize broadband detection with a small improvement in their performance but their integration not only increases the detection volume of these structures but also involves costly growth techniques [38]. The other drawback of these detectors are the instability in their noise performance which are limited by the temperature [37]. Apart from the above drawback of traditional broadband photodetectors they have some major limitations in the following aspects [26].

- Non uniformity
- Absence of band gap tunability
- Limited scalability
- Surface absorption
- Lattice mismatching
- No flexibility

Hence, to realize high-performance broadband photodetection, it is inevitable to integrate multiple photodetectors of various materials, which not only increases the complexity and volume of optoelectronic systems but also leads to exorbitant production costs. In addition, conventional photosensitive materials suffer from environmental toxicity, high-temperature processing, cryogenic working environment, poor flexibility, miniaturization difficulty by Moore's law, or complicated micro fabrication processes. For example, HgCdTe photodetectors require operating temperatures down to 70 K to achieve practical photo sensitivity, not to mention the environmentally unfriendly Hg/Cd element and the costly facilities for production, e.g., molecular beam epitaxy coupled with lattice-matched mono crystalline templates [26].

1.5 Needs of New Materials

The limitations of traditional materials with poor optical performance for modern optoelectronics and industrial broadband applications leads to the exploration of a new class of materials having high absorption coefficient, high thermal stability, large band gap tunability, high mobility, non-toxic, environment friendly and offers low-cost synthesis.

In recent years, low dimensional materials/ nano materials have been explored in recent optoelectronic applications due to their superior optoelectronic properties including strong light–matter interactions, thickness-dependent band gaps, high in-plane carrier mobility, flexible integrability, strong immunity to short channel effects, excellent stretchability/flexibility, high transparency, and high current-carrying capacity. In the context of photodetection via nanomaterials, 2D materials have proven themselves as potential candidates and have aroused considerable research enthusiasm from both academic and industrial communities [26]. A series of broadband photodetectors based on 2D materials have been explored and developed by various researchers to meet the ever-changing demands in various scenarios. For example, Yao *et al.,* [39] have achieved broadband photodetection ranging from 370 nm to 118.8 μm based on Bi_2Te_3/Si heterojunction. The broad range detection by Yao *et al.,* [39] have been achieved by combining the photo responses of Bi_2Te_3 for NIR–terahertz and Si for UV–NIR. Similarly, Xuechao-

Yu *et al.,* [40] have reported plasma treated bi-layer $PtSe_2$ with an effective wavelength range from 632 nm to 10 μm. Thus, it is potentially observed that the low dimensional materials and their hybrid combinations with other nanostructures have been spotted as the viable option to replace traditional materials for realizing an efficient broadband photodetector.

1.6 Nanostructures and their Classification

Nanomaterials or Low dimensional nanostructures are substances with at least one external dimension that measures in few nano-meters [41]. Recently, materials are the interest of study at nano scale due to their unique optical, electronic, and chemical properties in comparison to their bulk counterpart. The emerging properties of nanomaterials have proven their potentiality in optoelectronics, medicine, and other fields. Apart from various fields nanomaterials possess their potential impact in photodetection due to their, atomically thick geometry, high surface to volume ratio, strong light matter interaction, etc.

Based on the dimensions for which the motion of charge carriers is not restricted, nanomaterials are classified as zero-dimensional (0D), one-dimensional (1D), and two-dimensional (2D), while three-dimensional (3D) material represents the bulk state of materials. The schematic of the classification of nanomaterials are shown in Fig.1.8.

1.6.1 Zero Dimensional (0-D) Nanostructures

The semiconductor nanostructures in which the motion of carriers or excitons (Bound state of an electron-hole pair by the electrostatic Coulomb force) are confined in all three directions are called zero-dimensional (0D) nanostructures. The prominent example of the 0D nanostructure is quantum dots (QDs). In comparison to other nanomaterials, 0D QDs structure offers high absorption along with easy and low cost chemical route synthesis which enables them a potential contender for photodetection applications.

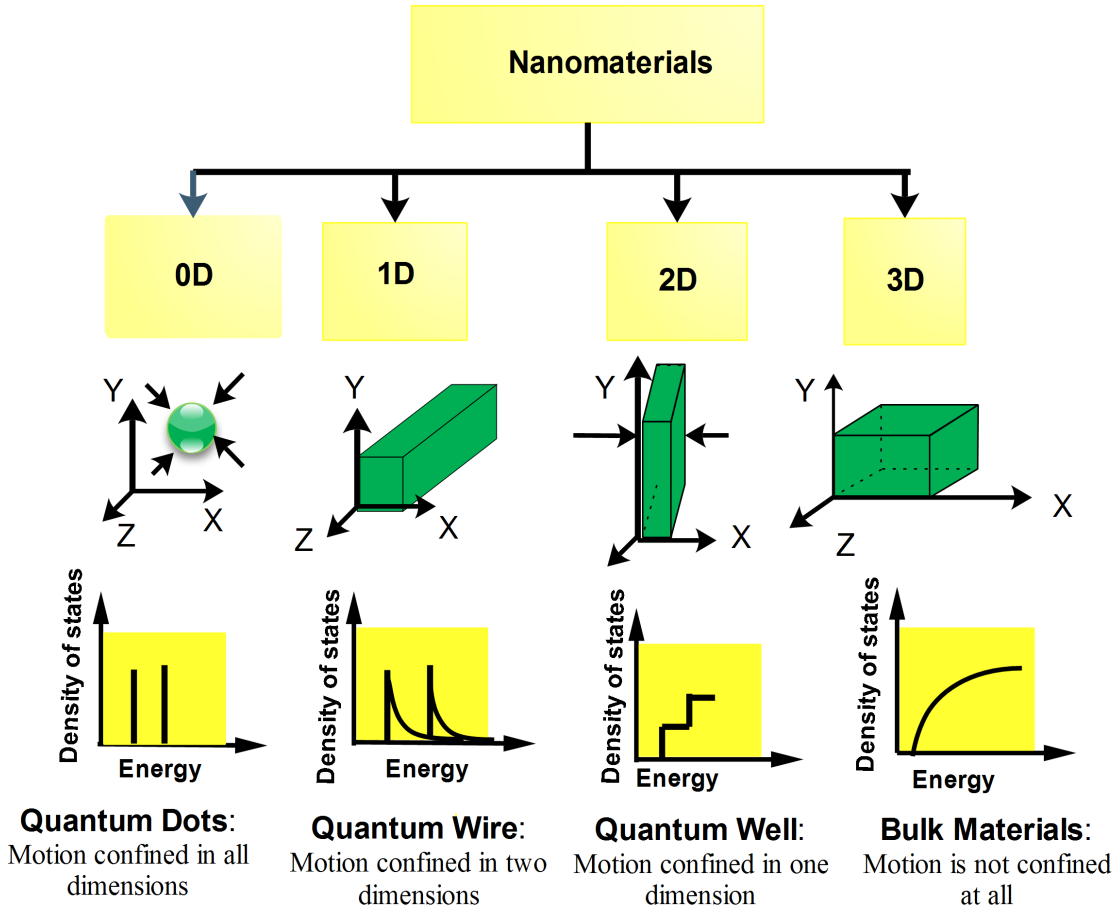

Figure 1.8: Classification of nanomaterials on the basis of their carriers motion restriction

1.6.1.1 Quantum Dots

Quantum dots are the intermediate state between bulk and a single atom material. Scaling down all the dimensions of bulk materials into a nanoscale region leads the formation of QDs structure. The scaling of materials into nanoscale bound the motion of the charge carriers and leads confinement effects. The confinement effects in nanostructure/QDs modify the electronic band structure of materials. When all the dimension of materials is scaled down less than the Bohr's radius the quantum confinement comes into the picture and discretize the energy levels in the valence and conduction band in comparison to bulk materials [42] as shown in Fig.1.9. The various parameters which defines the confinement of nano-structures or QDs are discussed below.

Quantum Confinement: Quantum confinement in nanostructure results when

any dimension of material goes in a nano region that is less than the Bohr radius of the materials. The size confinement in the materials leads to discretization in their energy levels in comparison to bulk materials. The quantum confinement principle of 0D-QDs structure is shown in Fig.1.9 (a). The confinement in size of materials increases the band gap of QDs in comparison to their bulk state which is inversely proportional to the size of nanostructure. The band gap of QDs structure over bulk materials are defined by Brus equation [43]

$$\Delta E(R) = E_g(R) + \frac{h^2}{8R^2}\left(\frac{1}{m_{e*}} + \frac{1}{m_{h*}}\right) - \frac{1.8e^2}{4\pi\epsilon_0\epsilon_\alpha R} \tag{1.15}$$

In the above equation, ΔE(R) is the new band gap energy of QDs due to confinement phenomenon, E_g(R) is the band gap energy of materials in their bulk state, h is the plank's constant, R is the radius of the particle, m_{e*}, m_{h*} are the effective mass of electron and hole respectively, ϵ_0 is the permittivity of a vacuum, ϵ_α is the high frequency dielectric constant, e is the charge of the electron.

Bohr's radius: When semiconductor materials are illuminated with photon energy the generation of electron hole pairs takes place. The set of these electron hole pairs is called excitons and treated as two bodies within the materials held together with Colombian interaction. The average distance between these excitons (electron-hole pairs) bounded with each other with Colombian interaction is called excitons Bohr radius as shown in Fig.1.9 (b). There is a defined limit of Bohr radius for each semiconductor structures and defined as [44]

$$a_b = \epsilon\frac{m}{m^*}a_0 \tag{1.16}$$

where, ϵ is the dielectric constant of the material, m^* is the mass of the particle, m is rest mass of electron, and a_0 is the Bohr's radius of hydrogen atom.

Density of State (DOS): The density of the state is an important parameter to study the basic electronic structure of materials. The density of state of the materials defines the number of allowed energy states for the charge carrier per unit volume of the materials. The density of state of QDs is discrete in comparison to the bulk materials

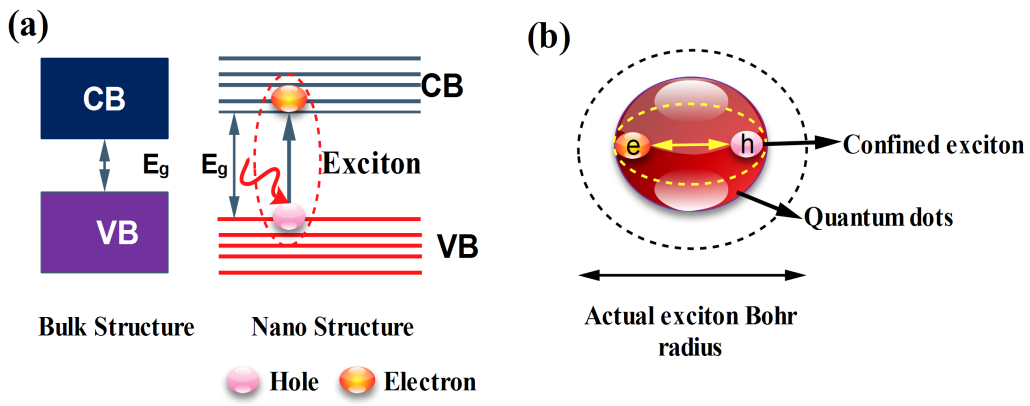

Figure 1.9: Principle of (a) Band gap engineering of QDs nanostructures over bulk materials (b) Quantum confinement effect

as shown in Fig.1.9 (b) due to confinement effects. The discrete energy levels in QDs make them a suitable contender in broadband optoelectronic applications where the transition from different sub bands has been used to detect a broad spectrum of light without integrating any other materials.

The trapping of excitons in all directions leads the QDs having dominated quantum confinement effects.The smaller change in the dimension/size of the QDs modifies the energy band of the materials more in comparison to other nanostructure i.e., 2D and 1D. The allowed energy bands of the confined excitons in the QDs can be approximate via a potential function V(r) of the particle inbox with the radius of the potential well is L is:

$$V(r) = \begin{cases} 0 & \text{if } r < L \\ \infty & \text{if } r > L \end{cases}$$

Now, the energy levels E_n in the quantum dot could be realized as[45]

$$E_n = \frac{\pi^2 \hbar}{2m^*}\left(\frac{n_x^2}{L_x^2} + \frac{n_y^2}{L_y^2} + \frac{n_z^2}{L_z^2}\right), \psi = \phi(x)\phi(y)\phi(z) \tag{1.17}$$

In the above expression, ϕ is the wave function of the charge carrier. n, L_x, L_y, L_z and $\hbar$ are the quantum number, particle confinement dimensions in x, y, z direction, and Planck's constant divide by 2π, respectively and ψ denotes the particle wave function.

The solution of above equation is valid only for single exciton. For the case of multiple exciton generation, there will be a Colombian interaction (E_c) between the charge pairs and could be approximate as:

$$E_c = k_e q^2 \left(\frac{1}{b_x} + \frac{1}{b_y} + \frac{1}{b_z} \right) \tag{1.18}$$

In the above equation k_e is the electron transfer rate and b is the natural separation of the electron and hole pair in x,y and z direction. By considering the Colombian interaction as per the literature [46], equation 1.17 can be modified as

$$E_n = \frac{\pi^2 \hbar}{2m^*} \left(\frac{n_x^2}{L_x^2} + \frac{n_y^2}{L_y^2} + \frac{n_z^2}{L_z^2} \right) - E_c, \psi = \phi(x)\phi(y)\phi(z) \tag{1.19}$$

From the above discussion, the bandgap of QDs is inversely proportional to their size and offers discrete energy levels in their electronic structure. Apart from this quantum dots also offer high surface to volume ratio over other nanostructures like 2D and 0D due to their nanostructure geometry.

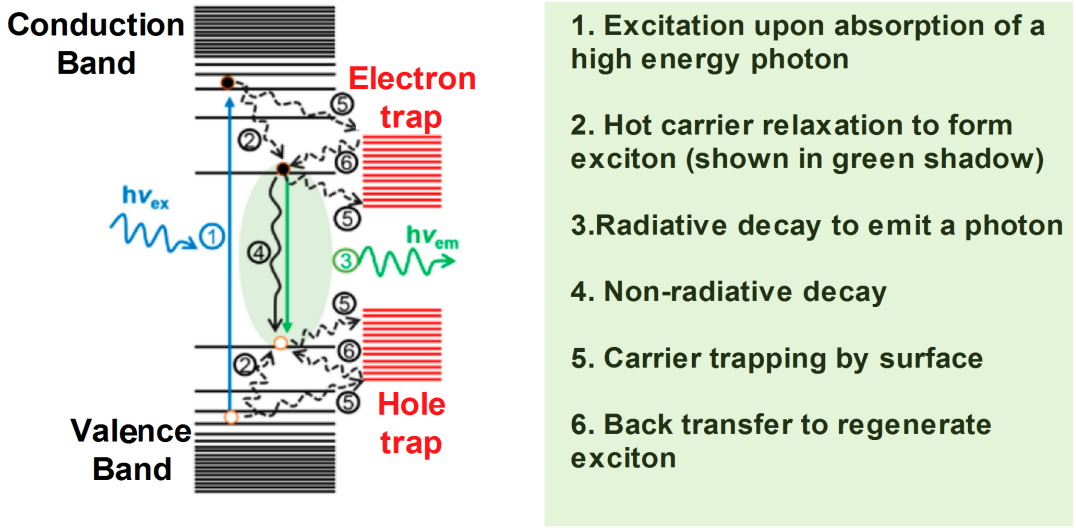

Figure 1.10: Scheme of the basic processes involving various excited states in a QDs upon photo-excitation

The high surface-to-volume ratio of the QDs structure facilitates a large exposed area for photons. The strong light to matter interaction in QDs makes them a suitable

contender for strong light absorber structure over bulk and other nanostructures. The confinement in the excitons in 0D nanostructure also increases the bandgap of materials in comparison to their bulk and other nanostructures. The size-dependent absorption and large bandgap tunability [42] in QDs structures make them a potential contender for broadband photodetection with the advantages of low-cost synthesis and low detection volume. The various process in the QDs structure under photo-excitation is shown in Fig.1.10 [47]. The sub-band carriers transitions along with charge trapping in the electronic structure of QDs make them curious structures for study under optical illumination.

1.6.2 One Dimensional (1-D) Nanostructures

The nanomaterials in which the motion of carriers are restricted in two dimensions while the charge carriers can freely move in their non-confined dimension. The energy band of 1D nanostructure, if the motion of excitons are bounded in x and y direction and they are free to move in the z-direction, is given by [45]

$$E_n(k_z) = \frac{\pi^2\hbar^2}{2m^*}\left(\frac{n_x^2}{L_x^2} + \frac{n_y^2}{L_y^2}\right) + \frac{\hbar^2}{2m^*}(k_z^2), \psi = \phi(x)\phi(y)exp(ik_z z) \tag{1.20}$$

The prominent example of the 1D nanostructures are nanowires, nanotube, and nanorods. The uniform 1D nanowires are having a wide range of applications in ultra fast photodetectors fabricated at the length of nanowires scale due to their ultra-high conductivity. Although having high conductivity, the nanowires photodetector suffers from inefficient charge transfer due to high scattering [48] which results from the non-uniformity of these nanostructures compared to 2D materials, therefore, and need well controlled and costly synthesis techniques to optimize their performance in optoelectronic applications.

1.6.3 Two Dimensional (2-D) Nanostructures

Two-dimensional materials are the best-known materials for optoelectronic applications. They offer a sheet-like nanostructure where the motion of carriers (excitons) are confined

in one dimension while they are free to move in other two-dimension. The confinement of the exciton in the one dimension is achieved by scaling the resultant dimension in nano regions. The confinement of the carriers in one dimension leads to the trapping of charge carriers in that dimensions and could be realized by a high potential barrier across the one dimension as shown in Fig.1.8. The change in any dimensions modify the electronic band structure of the materials and is estimated via an effective mass approximation model for the energy levels $E_n(k_y,k_z)$ inside the quantum well of size (L_x) as per literature [45]

$$E_n(k_y, k_z) = \frac{n^2\pi^2\hbar^2}{2m^*(L_x^2)} + \frac{\hbar^2}{2m^*}(k_y^2 + k_z^2), \psi = \phi(x)exp(ik_y y + ik_z z) \tag{1.21}$$

In the above expression, ϕ is the wave function of the charge carrier. n, k_y, k_z and $\hbar$ are the quantum number, wave vectors in y and z direction, and Planck's constant divide by 2π, respectively. From the above expression, it was noted that the size-dependent energies bandgap properties of 2D materials make them a potential contender for photodetection applications.

After the successful exploration of 2D-graphene from the bulk graphite in 2004 [49] 2D materials have been widely used in optoelectronic applications. Apart from their atomic thick dimension they provide large lateral area synthesis, high adhesiveness and simple stacking with other nanostructures [50]. The prominent example of 2D materials is graphene which offers ultra-high mobility of the order of 10^5 cm^2/V-s [23]. Therefore, graphene offers ultra-fast photodetector structures but suffers from low absorption which degrades the performance of graphene detectors in terms of their other optical property like responsivity, sensitivity, etc.[23] The high improvement in the performance of graphene-based detectors has been realized by integrating it with other nanostructures like QDs which offers a higher absorption coefficient [51, 23, 52].

1.6.4 Merits of Quantum Dots (0D) and 2D-Nanostructures

As per the above discussions, the nanostructures offers large advantages over the bulk materials due to their size dependent tunable optoelectronic properties which alters the

band gap of nano-materials as per the desired applications.

Quantum dots structure processes ultra high absorption among all nanostructure due to their confinement in all direction while 2D materials offers high lateral area, smooth surface, high adhesion and compatibility with various substrate and nanostructure due to their weak Van-der Waals forces in out of plane directions [53]. These emergent properties of 0D and 2D materials make them a potential contender materials for broadband photodetection. Accordingly, in this thesis we have studied 0D, 2D and their hybrid (0D/2D) nanostructures for broadband photodetection.

1.7 Synthesis of Nanostructures

The nanostructures synthesis has two approaches: (1) Top-down approach-where a large bulk materials is broke-down into a nano materials and (2) Bottom-up approach which involves the assembly of atoms and molecules to generate a nanomaterials. The schematic of top-down and bottom-top approaches are shown in Fig.1.11.

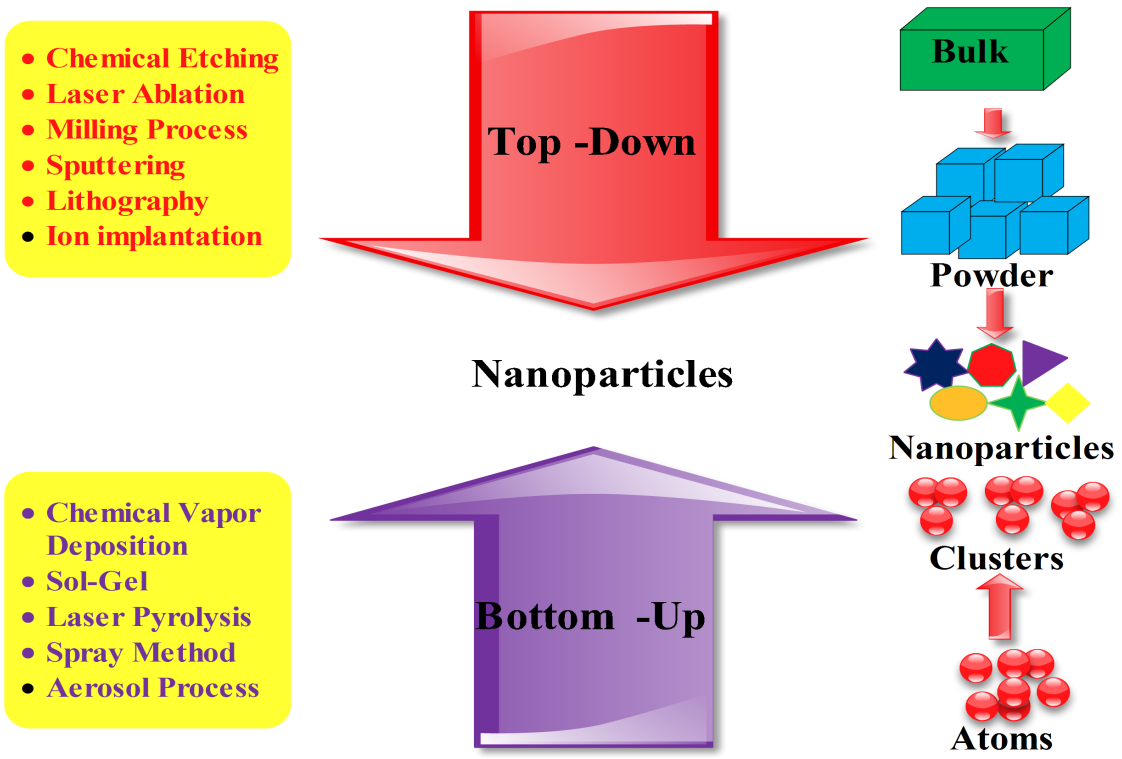

Figure 1.11: Synthesis process of nanostructures: Top-down and Bottom-top approach

1.7.1 Top-Down Approach

In the top-down approach, a larger metal is used for the production of nanoparticles by a physical method via the mechanical breakdown of the large metal structure. It is an economic, energy demanding, and lengthy process [54]. The top-down approach begins with the bulk counterpart that leaches out systematically bit-after-bit, leading to the generation of fine nanoparticles. Several physical methods are adopted for the mass production of nanoparticles such as photo-lithography, electron beam lithography, milling techniques, anodization, and ion and plasma etching [55].

☛: The biggest problem with top-down approach (physical methods) is the imperfection of the surface structure. Such imperfections would have a significant impact on the physical and chemical properties of nanostructures/nanomaterials [56, 57].

1.7.2 Bottom–Up Approach

The bottom-up approach involves assembling atoms and molecules to generate a diverse range of nanoparticles. Examples of the bottom-up approach include self-assembly of monomer/polymer molecules, chemical or electrochemical nanostructural precipitation, sol–gel processing, laser pyrolysis, chemical vapor deposition (CVD), plasma or flame spraying synthesis, and bio-assisted synthesis [58, 59]. Bottom-up approach is the most common approach that has been used to synthesize the QDs, 1D, and 2D nanostructures due to its well control over parameters like thickness, morphology, particle size etc.

☛: The potential advantages including low defects along with homogeneous chemical composition of bottom-top approach [56, 57] motivated us to involve this approach for the synthesis of nanostructures i.e., 0D-CTS QDs, 2D-graphene and 2D-SnS_2 used in this thesis work.

1.8 Characterizations Techniques for Nanostructures

There are various techniques which have been used to confirms the structural phase, morphology, size of nanomaterials, thickness, and elemental composition of nanostructures. The small size of nanomaterials needs special characterizations tools with high resolution to study the structure of nanomaterials at this scale. Some widely used structural and optical characterizations techniques of nanostructures have been reported here briefly.

1.8.1 Structural Characterizations Techniques

1.8.1.1 X-Ray Diffraction (XRD)

X-ray diffraction (XRD) is used for the structural analysis of materials. The high-energy X-ray of an appropriate wavelength is used to study the structural pattern of samples by collecting the scattered X-ray coming from the sample. The X-ray diffraction analysis has been used to measure the crystal structure, plane orientation, and nature of the sample i.e., crystalline, poly-crystalline or amorphous. The XRD has also been used to determine the phase composition in the structure, qualitative phase analysis, parameters of a unit cell in structure, crystalline micro-strain, and texture, and also the residual stress in the samples. The main component of the XRD system is an X-ray source, goniometer, sample holder, radiation detector, and a single processor and readout. The working principle of X-ray diffraction is shown in Fig.1.12. When high-energy electrons strike an anode in a sealed vacuum chamber, X-rays are generated. The generated high-energy X-rays are then focused towards the sample by using a lead screen. The specific crystal structure of the sample materials the X-ray diffracted from the analyzed sample and form a photographic image on a photographic plate. The diffraction analysis of X-ray beams has been given by Bragg's equation. Bragg's equation gives the condition ($n\lambda=2dSin\theta$) [60] for a constructive equation that exists when the path difference equals some integral multiple of wavelength between the reflected X-rays from the analyzed

sample. Where, λ is X-ray wavelength, d is the plane spacing and θ is the angle of incidence.

The XRD have major advantages over other structural characterizations techniques. XRD is a fast technique to study the crystal structure of materials and the preparation of XRD sample is very easy. It facilitates computer-aided materials identification and is having a large library of known crystalline structures.

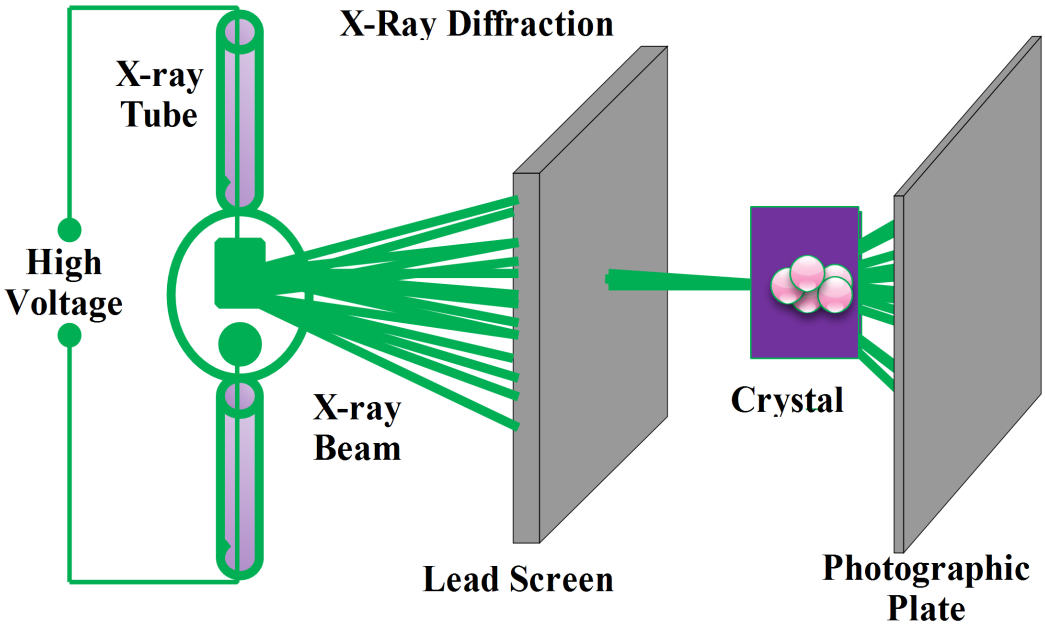

Figure 1.12: X-ray diffraction: Principle of operation with basic components

1.8.1.2 Transmission Electron Microscopy (TEM)

Transmission electron microscopy (TEM) is the best known structural characterization technique for nanomaterials. Nanomaterials with a size less than 1 nm could also be studied through this technique due to their high-resolution capability. The TEM analysis is mostly used to determine the shapes, size and inter planner spacing in the nanostructures by transmitting an electron beam through the samples. All 0D, 1D, and 2D nanostructure have been characterized by this technique to provide the strong potentiality in the characterization of QDs nanostructure. The basic working principle

of TEM is shown in Fig.1.13. The basic component of TEM consists electron gun, illumination system, sample holder, imaging system, and a viewing chamber. In a TEM setup, an electron gun is used to generate a high-energy electron beam focused toward the ultra-thin sample need to characterize. The transmitted beam from the sample is then focused on a fluorescent beam to create the imaging of the sample. In the TEM setup as shown in Fig.1.13 the condenser lenses used in various stages are used to control the amount of illumination or brightness that reaches or comes from the sample. The Objective lens has been used to focus the electron beam onto the sample and applies a small amount of magnification. The intermediate and projector lenses magnify the beam and project it onto the camera or screen to form an image.

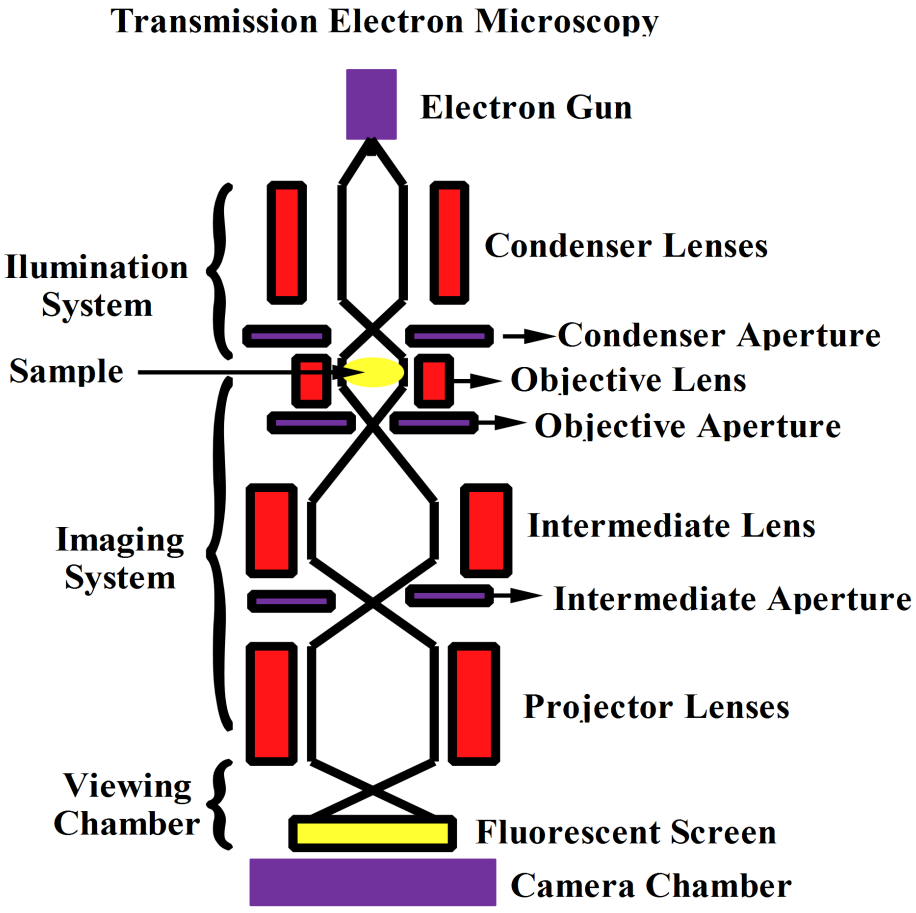

Figure 1.13: Basic principle of transmission electron microscopy (TEM)

The TEM offers very powerful magnification and resolution and provides detailed information of an element and compound structure. It has few drawbacks which include

laborious sample preparation, samples are limited to those that are electron transparent and require special maintenance for proper operation.

1.8.1.3 Scanning Electron Microscope (SEM)

The Scanning Electron Microscope (SEM) have a similar kind of setup as TEM analysis with the difference that in this technique the image of the sample is formed by recording the scattering of secondary electrons from the surface of the sample. The SEM technique is used to study the surface morphology of nanostructure along with their elemental composition. The basic setup of the SEM is shown in Fig.1.14 and having the same set as TEM but having two more components i.e., secondary electron (SE) detector and back scattered electron (BSE) detector. The main advantage of SEM analysis in comparison to TEM analysis is that it provides the surface morphology of nanostructure due to the scattering of the secondary electrons from the sample. The energy of the secondary electrons, generated from the various depth of the sample has been measured by the SE detector and the analyzed energies of these electrons have been used to create the SEM image on the screen. The SEM analysis of the samples suffers from electrostatic charging, surface damaging, thermal damaging, etc., which are the measure issues in this technique and could be controlled by coating a conducting film over the sample before the SEM analysis performed.

1.8.1.4 Atomic Force Microscopy(AFM)

The atomic force microscopy technique has been used to measure the lateral as well as horizontal dimensions of the samples. It works on the principle of atomic force experienced between the sample and the tip of the cantilever. The interaction of the sample with the tip of cantilever provides a 3D image of any nanostructure. On the basis of the cantilever tip interaction with the sample, there are basically three modes of operation used in AFM technique named as contact mode, non-contact mode, and tapping mode. The basic principle of the AFM technique is shown in Fig.1.15. The basic component of AFM consists of a laser source, a cantilever along with cantilever tip, and a quadrant photodetector to create the picture of the sample. When a cantilever

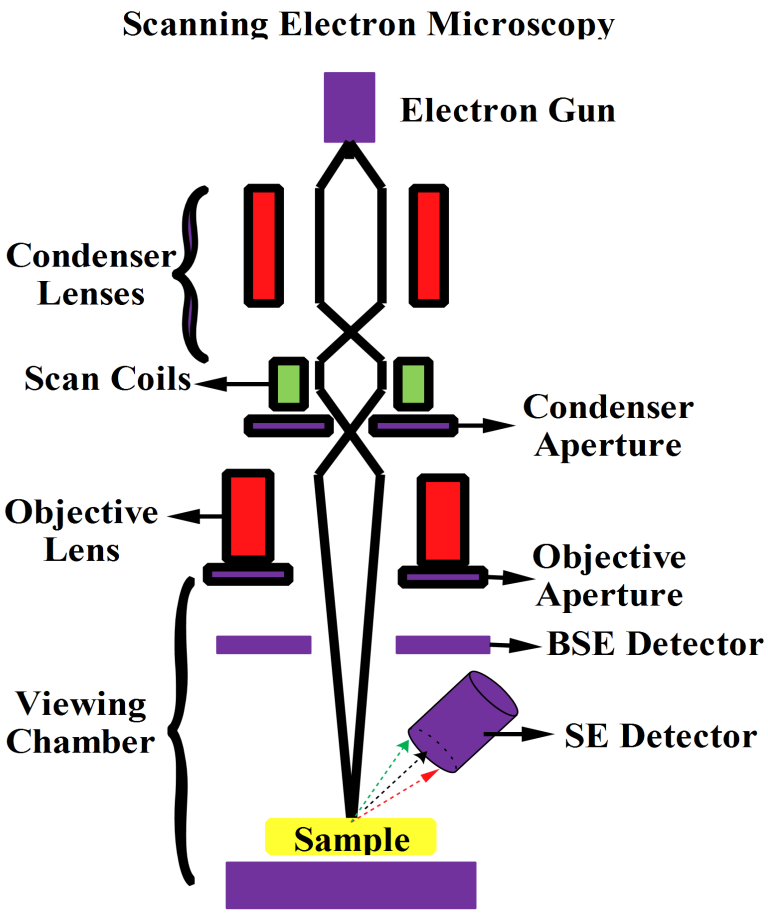

Figure 1.14: Basic principle of scanning electron microscopy (SEM)

tip comes in the contact with the sample there exists force on the AFM cantilever rod as per the morphology of the sample surface. Since, there is a laser source focused on the top of the cantilever beam as shown in Fig.1.15 the reflected laser beam from the cantilever top is also deflected and recorded by the quadrant photodetector to record all defection of the beam in all directions and create the 3D image of the sample. AFM is mostly preferred to estimate the height of nanostructure material over other structural characterization techniques due to its high vertical resolution and it also give information about the horizontal direction of sample. In comparison to all other working modes of AFM, contact mode are treated to be more accurate and give resolution in the 3D AFM image with high accuracy. Even having a good resolution, contact mode may leads the damaging of sample surface. The other modes with sufficient 3D resolution, called non-contact and tapping mode, are preferred in the scenario where the damaging

of the nano-structural surface is the primary issue.

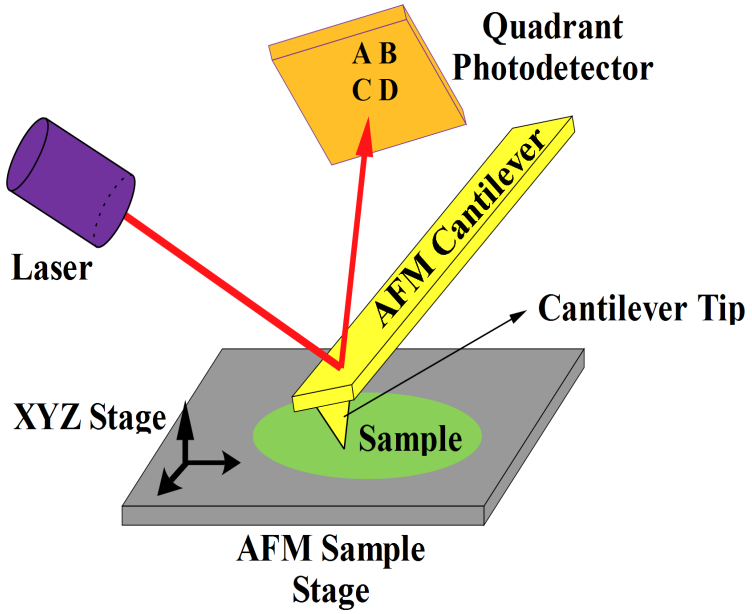

Figure 1.15: Basic principle of atomic force microscopy (AFM)

1.8.1.5 Raman Spectroscopy

Raman spectroscopy is a spectroscopic technique typically used to determine vibrational modes of molecules, although rotational and other low-frequency modes of systems may also be observed. Raman spectroscopy is commonly used in chemistry to provide a structural fingerprint by which molecules can be identified. Typically, in Raman spectroscopy a sample is illuminated by a laser beam with a incident/excitation frequency (v_o) and results an internal molecular vibration in sample having frequency (v). Due to internal molecular vibration in sample the scattered light coming from the sample will having three component of frequencies. The first frequency component with no change from the excitation frequency of the laser source. On the other hand, there are two other scattered waves one is having a frequency (v_o+v) and the other is having frequency (v_o-v) components. The shift in the frequency of the excitation light is called the Raman scattering phenomenon. The sifting in the frequency is treated as a Raman shift and used to rapidly characterize the chemical composition and structure of a sample, whether solid, liquid, gas, gel, slurry or powder by observing the Raman

spectra. The schematic of the principle of Raman spectroscopy is shown in Fig.1.16.

Raman spectroscopy has also been used to determine the molecular concentration in the sample and used to characterize the sample qualitatively and quantitatively. The peak's intensity observed in the Raman spectra is used to determine the number of layers in the characterized materials. Most of the layered materials like graphene, MoS_2, WS_2, etc., have been characterized by Raman spectroscopy to analyze the number of layers and also the defects in the nonstructural arises during the synthesis process [2].

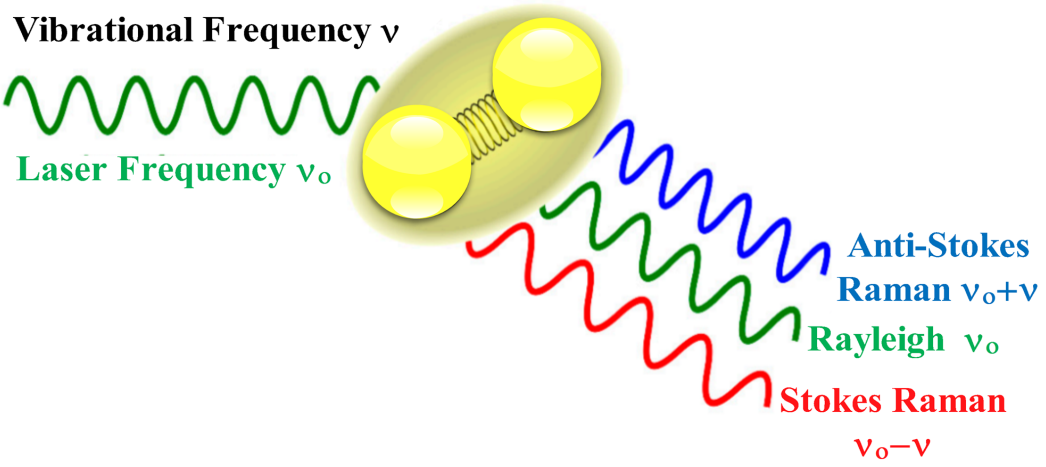

Figure 1.16: Basic principle of Raman spectroscopy (From Ref. [2])

Raman shifts are typically reported in wave-numbers, which have units of inverse length, as this value is directly related to energy. To convert between spectral wavelength and wave-numbers of a shift in the Raman spectrum, the following formula can be used [61].

$$\Delta \upsilon \ = \left(\frac{1}{\lambda_0} - \frac{1}{\lambda_1} \right) \tag{1.22}$$

where $\Delta \upsilon$ is the Raman shift expressed in wave number, λ_0 is the excitation wavelength, and λ_1 is the Raman spectrum wavelength.

1.8.2 Optical characterizations Techniques

There are various optical characterizations techniques used to know the optical response of nanomaterials. Here some prominent techniques to study the optical response of nanomaterials are discussed.

1.8.2.1 Spectroscopic Analysis (UV-Visible-NIR Spectroscopy)

The UV-Visible-NIR spectroscopy is used to measure the absorption spectrum of the given sample. The spectroscopy work on the principle of transition of the electrons within molecule or ions. UV-Visible-NIR spectroscopy helps in the qualitative and quantitative study of matter. The principle of operation of UV-Visible-NIR Spectroscopy is shown in Fig.1.17. In Fig.1.17, a light source is used to illuminate the sample, here a prism or wavelength selector is used to illuminate the resultant sample with a specific wavelength and the interaction of light with the sample take place. The interaction of light with the sample leads to two processes light scattering and light Absorption. The interaction of radiation with matter depends upon both radiation properties and structural parts of the materials involved. This interaction between matter and radiation leads to a variety of spectra measured with the help of a detector. Two types of the spectrum are measured through this spectroscopy one is emission spectroscopy and the second one is absorption spectroscopy.

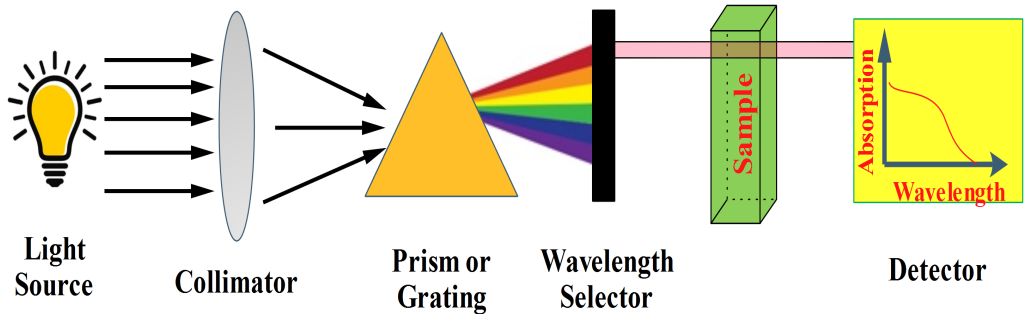

Figure 1.17: Basic principle of UV-Visible-NIR spectroscopy

When the atoms or molecules for the given sample are subjected to heat or electric discharge, they absorb energy and exited. In the excitation process, the electron tran-

sition from the ground state to the excited state takes place. Since it is known that the excited electron having a very short period in their excited state so they return to their lower state and so the energy absorbed in the sample is released as light energy. When this energy passes through the prism, it gives rise to an emission spectrum. while on the other hand in absorption spectroscopy when electromagnetic radiation is passed through a solution, some of it is absorbed, some are reflected and the remainder is transmitted. When this transmitted light passed through a prism an absorption spectra is obtained.

1.8.2.2 Photo-Luminescence (PL)

Photo luminescence (PL) is the emission of light that is caused by the irradiation of a substance with other light. The term embraces both fluorescence and phosphorescence, which differ in the time after irradiation over which the luminescence occurs. In a typical PL experiment, a semiconductor is excited with a light source that provides photons with an energy larger than the bandgap energy. Once the photons are absorbed, electrons and holes are formed with finite momenta in the conduction and valence band, respectively as shown in Fig.1.18. The excitation then undergoes energy and momentum relaxation towards the band gap minimum.

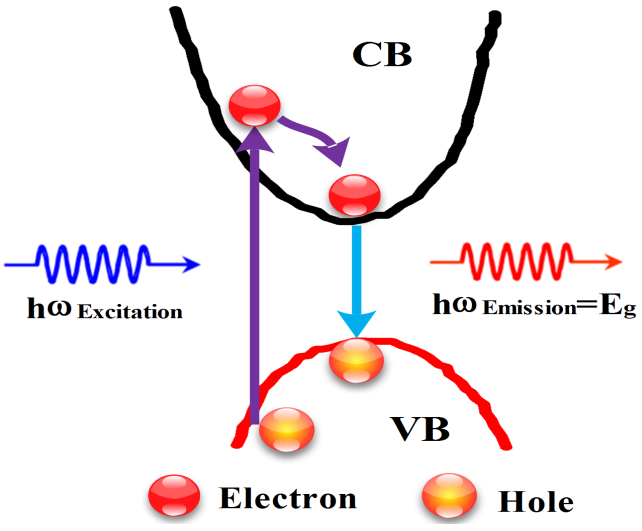

Figure 1.18: Basic principle of photo-luminescence (PL) process

PL measurement in a semiconductor material is used to analyze the steady-state, time resolve spectra, PL decay, PL quantum efficiency, and also confirm the radiative characteristics of semiconductors.

1.8.3 Electrochemical Characterization Technique

1.8.3.1 Cyclic Voltammetry (CV)

Cyclic Voltammetry (CV) is an electrochemical technique that measures the current that develops in an electrochemical cell under conditions where voltage is more than that predicted by the Nernst equation [62]. CV is performed by cycling the potential of a working electrode and measuring the resulting current. The detailed working principle of Cyclic voltammetry has been explained in literature [62]. In brief the estimation of electrochemical band gap via CV measurement is done by using three electrodes dipped into a electrolyte solution [7]. The three electrodes in the CV setup are named as working electrode, counter electrode and reference electrode. The band gap of semiconductor materials is measured after drop casting the sample onto the working electrode. After drop casting the sample, the hopping of voltage in a small step size is performed and the corresponding current is measured. The generated closed voltage vs current plot or CV scan, gives the reduction and oxidation peaks of the sample. The obtained reduction and oxidation peaks in CV scan are used to find out the electrochemical band gap for the sample with the help of well-known CV equations as discussed in various reports [7, 63, 23].

Apart from estimating the band gap, CV has become an important and widely used electro-analytical technique in many areas of chemistry. It is often used to study a variety of redox processes, to determine the stability of reaction products, the presence of intermediates in redox reactions, electron transfer kinetics, and the reversibility of a reaction. CV can also be used to determine the electron stoichiometry of a system, the diffusion coefficient of an analyte, and the formal reduction potential of an analyte, which can be used as an identification tool.

1.9 Introduction of Cu_2SnS_3 (CTS) and 2D-Materials

In this section, the electronic and optical properties of 0D nanostructure and 2D materials which are synthesized and characterized in this thesis are reviewed. The optical and electronic properties of CTS QDs (0D), high mobility 2D-graphene and a low dimensional SnS_2 have been studied sequentially.

1.9.1 Cu_2SnS_3 (CTS) and its Nanostructures

Cu_2SnS_3 is a newly explored nontoxic compound materials used in Vis-NIR optoelectronic applications [7, 64, 63]. The non-toxic and earth-abundant nature of CTS over other widely used Vis-NIR active materials like PbS, PbSe, HgTe, CdTe, etc., [63] make it a potential contender for the Vis-NIR active material. CTS offers high absorption coefficient and large bandgap tunability in its nanostructure [63]. Because of the above properties, CTS and its QDs structures are widely used in photocatalysis, light-emitting diodes, nonlinear optics, and photodetection, etc. [65, 66] The various methods has been explored to synthesize the nanostructure including physical as well as chemical methods for enabling their potential application in optoelectronics. Physical methods like ball milling are unsophisticatedly resulting in irregular morphology, and also correspond to crystals with numerous defects. Moreover, other physical methods are expensive and the necessity of vacuum adds to the cost of synthesis. Chemical methods provide better yield and are easy to synthesize the nanostructure with better morphology control. Chemical methods including one-pot chemical synthesis, hot injection, solvothermal, hydrothermal, and microwave irradiation produce nanostructures with tunable sizes, shapes, chemical compositions, and phases. Out of mentioned chemical root synthesis of nanomaterials, the solvothermal technique has been used extensively due to its fine control over size as well as morphology of the nanostructures derived [67]. The best control in the morphology and the size of solvothermal synthesized CTS nanomaterials have shown a wide range of applications both in material science as well as in optoelectronic applications [67, 5]. In Table-1.3 we have highlighted the structural, optical, and electronic parameters of the CTS and its nanostructures.

1.9.1.1 Electronic Property

The electronic parameters of CTS and its nanostructures (QDs) has been studied by the various researchers (Table-1.3). The available literature on CTS nanostructure confirms the potential applications of this materials for visible-NIR photodetection with good optical characteristics [5]. The QDs structure of CTS having band gap variation from 0.93 to 1.77 eV and the absorption coefficient of $10^5 cm^{-1}$ make it a suitable contender for broadband (vis-NIR) photodetection and photovoltaic applications [5]. The nanostructure of CTS having hole concentration of 10^{18} cm^{-3}, hole mobility of 1-80 cm^2/V-s and electrical conductivity of 0.5-10 S/cm have been reported in literature [64]. Apart from the superior as well as favorable optoelectronic properties of CTS nanomaterials, it also involves the simplest synthesis techniques as discussed in various reports [5, 7, 63]. CTS and its nanostructures can be grown by simple and low-cost techniques like spin coating, dip coating, spray coating, and screen printing which can be used for large area coatings thus overcoming the cost and formation of secondary phases associated with vacuum-based techniques.

Table 1.3: Some Typical Properties of Cu_2SnS_3 Nanostructures

Parameters	**Values**
Energy Gap and Type	0.93 to 1.77 eV, p-Type [5]
Absorption Coefficient	10^4–10^5 [63]
Exciton Bohr's radius	2.5–4.6 nm [68]
Density	5.02 g/cm^3 [69]
Crystal Structure	Cubic, Tetragonal, Wurtzite, Monoclinic, Hexagonal[3]
Melting Point	837^0C
Lattice Constant	a = 5.41 Å, b=5.41 Å, c = 10.83 Å (Tetragonal Phase Structure) [63, 70]
Hole mobility	1–80 cm^2/V-s [63]
Thermal Conductivity	2.80 W/mK
Stable Phase at 300 K	Cubic, Tetragonal, Wurtzite [3]
Intrinsic Carrier Concentration	2.81×10^{21} cm^{-3} [63]
Electric Conductivity	0.5–10 S/cm [63]

- **Crystal Structure:**

In the structural study of CTS various research have been carried out to study the various atomic compounds of Cu, Sn and S and their phase structures. Cu-Sn-S exhibit many stable phases like Cu_2SnS_3, Cu_2SnS_4, Cu_4SnS_4, $Cu_2Sn_3S_7$, and $Cu_5Sn_2S_7$ among which Cu_2SnS_3 (CTS) has shown efficient photodetection properties due to its strong light matter interaction along with wide range of stability [3, 71, 7]. In addition, CTS have wide stability range and be devoid of Fermi level pinning while other forms exhibit poor hole-mobility and fermi level pinning [3, 71]. The non-toxicity as well as high absorption coefficient of CTS nanostructure leads our study more focused for photodetection applications [63, 7]. In Fig.1.19 the various phase structure of CTS has been discussed on the basis of atomic arrangement of Cu, Sn and S [3]. It is concluded that the high optical efficiency of Cu_2SnS_3 over other phases make it suitable contender for photodetection. In a review report [3] of CTS materials the authors has discussed the phase structure, band structure, electronic properties as well as the optical response of the CTS under light illumination. There are mainly five Crystallographic structures of Cu_2SnS_3 named as Monoclinic, Cubic, Wurtzite, Tetragonal, and Hexagonal as denoted in Fig.1.19 (a), (b), (c), (d) and (e), respectively.

In the thin film and bulk forms, only cubic, tetragonal and triclinic poly-crystalline morphology are formed [3, 72, 73]. Whereas in the nanocrystal form CTS exhibits crystalline phase structures named as wurtzite and hexagonal [74, 75]. The unit cell of monoclinic-CTS contains 24 atoms and theses atoms i.e., Cu, Sn, S occupy 4a Wyckoff position [3]. Further, four cations (Cu and Sn) are tetrahedrally bonded with S ions as in zinc-blend structure [76]. In cubic CTS structure, Cu, Sn, and S atoms occupy the 4b, 4a, and 24g Wyckoff positions, respectively [77]. In case of wurtzite-Cu_2SnS_3, both Cu and Sn atoms occupy the same Wyckoff position (2b), and the occupancy possibilities of Cu and Sn atoms are 2/3 and 1/3, respectively as shown in Fig.1.19. On the other hand, the crystallographic structure of hexagonal-Cu_2SnS_3 is similar to the α-CuSe structure. The hexagonal-Cu_2SnS_3 can be obtained by replacing of Cu(1), Cu(2), and Se atomic position with the Cu, Sn, and S, respectively. While in tetragonal phase structure CTS, the Cu atoms occupy the 4d, 2b and 2a Wyckoff position, Sn atoms occupy the 2b and 4d Wyckoff positions and S atoms situated in the 8i Wyckoff position [78, 4]. The bond

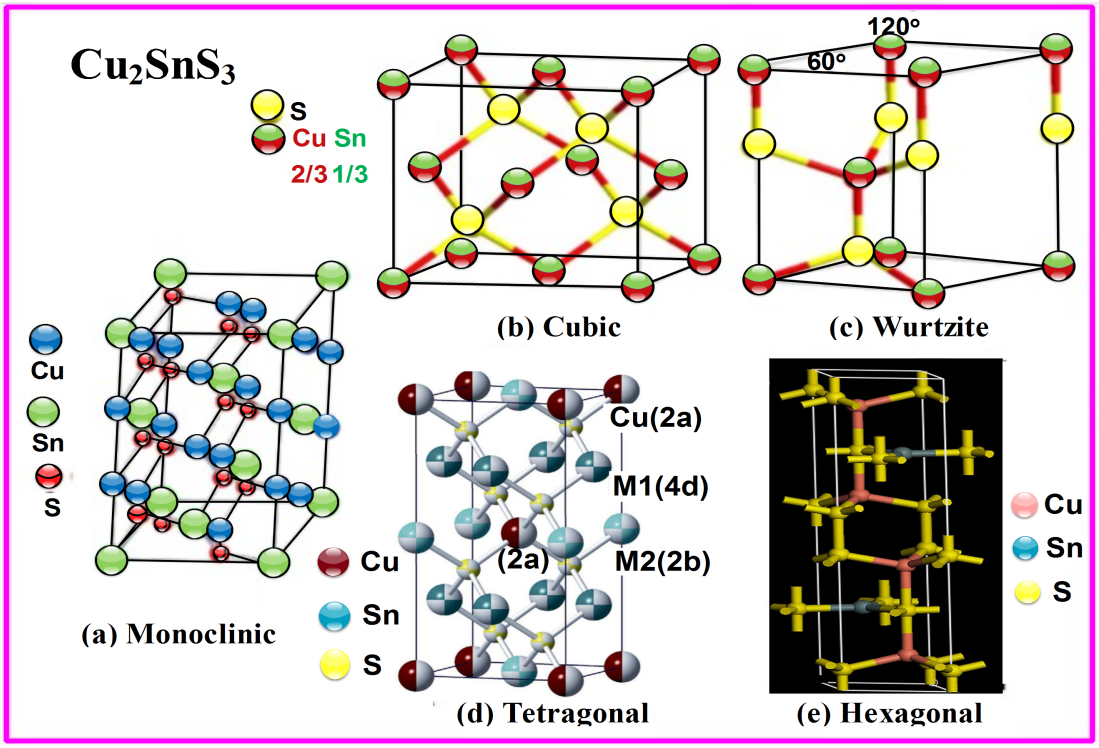

Figure 1.19: Crystallographic structures of Cu_2SnS_3 (a) Monoclinic, (b) Cubic, (c) Wurtzite, (d) Tetragonal, and (e) Hexagonal (From Ref. [3, 4])

length of tetragonal CTS has been further discussed in literature [79]. The cations i.e., Cu and Sn distribution are found to be in ordered form in monoclinic-CTS while tetragonal as well as the cubic structure having disordered position of these cations. The most important structures widely observed in nanostructures of CTS are wurtzite, hexagonal and tetragonal. Out of these three phase structure the tetragonal phase of CTS has been observed while realizing its QDs geometry by low cost solution processed techniques named as hydrothermal and solvothermal [5, 7]. Apart from this in the context of the energetically stable phases at low temperature ranges (25-780^{o}C), CTS exhibits tetragonal phase structure [3]. The temperature dependent phase variation in the other phase structures of CTS could be further studied from the extensive review reports [3, 72, 80].

- **Band Structure:**

It was noted that the band energy of nanomaterials is highly dependent on the crystal structure and defects in the materials. The various researcher has tried to explore

a the bandgap of CTS for various phase structures as reported in review literature [3]. In the review report, the valence band maxima (VBM) of CTS is formed mainly by the anti-bonding component of the hybridization between Sn-s and S-s states. In the further study, the conduction band minima (CBM) and valence band maxima (VBM) occur at the Γ-point, which indicates the direct optical transition nature in Cu_2SnS_3. In the mentioned review report [3] the authors have theoretically calculated direct bandgap energy of monoclinic form of Cu_2SnS_3, where the CBM and VBM occur at the Γ-point, which also indicates the direct optical transition nature in Cu_2SnS_3. Theoretically calculated direct bandgap energy of monoclinic Cu_2SnS_3 was 0.84 eV with the Heyd–Scuseria–Ernzerhof (HSE) function [76], 0.88 eV using HSE with a larger Hartree–Fock exchange contribution [81], and 0.63 eV with a beyond density functional theory (DFT) approach [8]. All these calculations showed single absorption for monoclinic Cu_2SnS_3. However, the experimental results [3] showed the double absorption onset of 0.90-0.93 eV and 0.97-1.02 eV from both optical absorption and quantum efficiency measurements. Further, Wild *et al.,* [82] reported that the double onset is an intrinsic feature of monoclinic Cu_2SnS_3. Recently, Andrea *et al.,* [83] explained this double onset phenomenon with experimental evidence and theoretical calculations. From the report, [3]) the energy gap between the first VBM (v1) and CBM is directly associated with the first absorption onset. Further, the second VBM (v2) and third VBM (v3) have maxima also at the Γ-point with the energies 0.12 and 0.16 eV below the VBM. These two bands, are thus responsible for the second absorption onset. On the other hand, the electronic band structure for other structures such as cubic-Cu_2SnS_3, wurtzite-Cu_2SnS_3, triclinic-Cu_2SnS_3, and tetragonal-Cu_2SnS_3 are insensitive to the cation distribution according to Zhai *et al.,* [76].

1.9.1.2 Optical Property

Cu_2SnS_3 has a bandgap of approximately 1 eV, an absorption coefficient between 10^4 cm^{-1} to 10^5 cm^{-1} and conductivity between 0.5 and 10 S/cm, which correspond to a hole concentration of 10^{18} cm^3 and mobility between 1 and 80 cm^2/V-s [64]. The reported absorption coefficient of CTS QDs is found to be far better in comparison to

other similar range photodetection materials like PbS, PbSe, HgTe, etc. The optical activity wavelength region of CTS QDs materials over other widely used Vis-NIR QDs structures are shown in Fig.1.20. The non-toxicity of CTS QDs over the PbS, PbSe, and earth-abundant and inexpensive qualities over In, Te materials, lead this nano-structure a better choice for Vis-NIR photodetection.

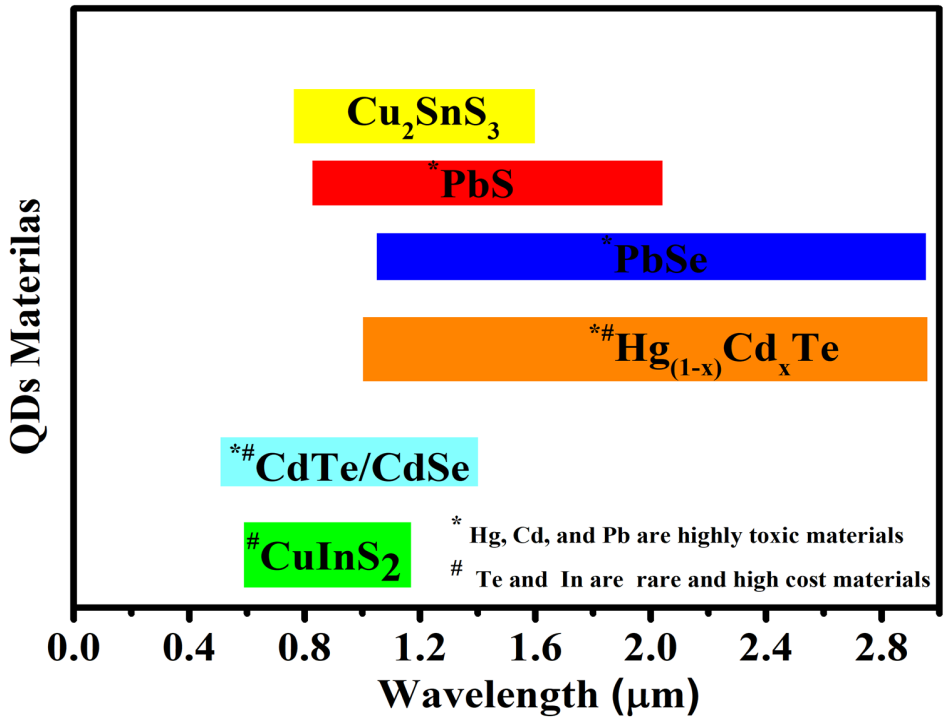

Figure 1.20: Optical spectrum of various QDs materials over CTS QDs (From Ref. [5, 6, 7])

The higher absorption of the synthesized CTS QDs structures has been reported by many researchers [5, 7]. The strong absorption of the CTS QDs structure has been achieved due to the high surface-to-volume ratio of QDs nanostructure over other structures like nanosheets, nanorods, etc. The CTS nanostructures exhibit particles size dependent electronic and optoelectronic properties [63, 5, 7]. The strongest optical absorption, as well as large particle size-tunable property of CTS QDs, have been utilized to realize a broadband photodetectors.

Fig.1.21 (a) shows the absorption spectra of Cu-Sn-S based stable phases (bulk) and their band-gaps [8]. The result shows the highest absorption coefficient for Cu_2SnS_3 structure with the bandgap estimated as 0.68 eV. Similarly, in the literature [63] the

thin film of CTS has been synthesized with the absorption coefficient 10^4 cm^{-1} and the bandgap of 1.23 eV. In the next phase, the same researcher group has synthesized the CTS QDs structure and studied their optical characteristics by changing the physical parameters like temperature, reaction time, etc. The band gap of CTS QDs varies between (0.93–1.77 eV) and the absorption coefficient is high (>10^4 cm^{-1}) [5]. Fig.1.21 (b) shows the absorption spectra of solvothermal synthesized CTS QDs [5]. The absorption spectra of the QDs structure show the broad light absorption of these materials from the visible to NIR range. The large absorption in the absorption spectra confirms the various size of CTS QDs which allows multiple sub-band transitions in QDs structure due to their discrete energy levels. Furthermore, the large size variation in the CTS QDs has been observed in study [7] which opens the way for exploring this material for broadband applications. The above-mentioned and explored strong optical characteristics of CTS nanostructure along with earth-abundant and non-toxic beauties make this material a suitable choice for Vis-NIR broadband photodetection applications.

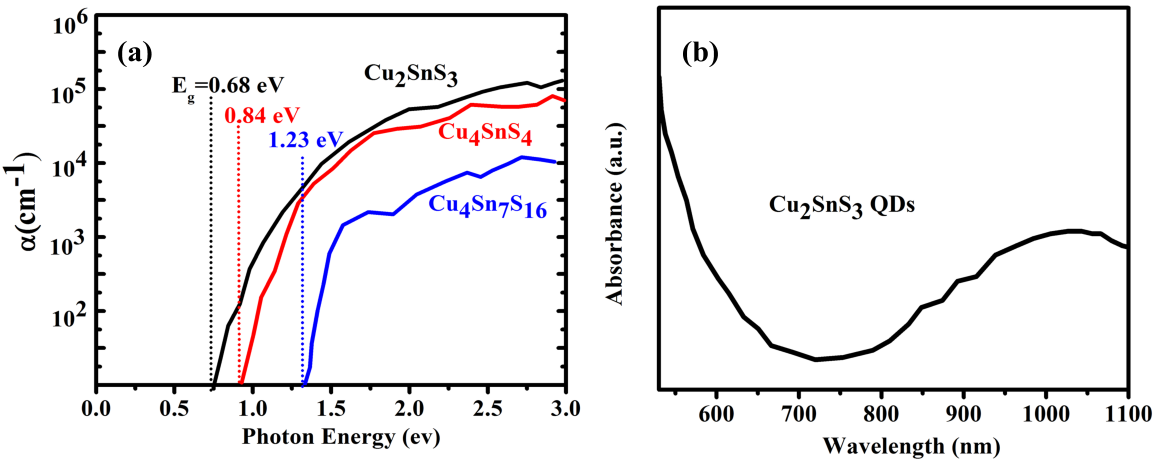

Figure 1.21: (a) Absorption coefficient of Cu_2SnS_3 (From Ref. [8]) (b) Broad absorption spectrum of CTS QDs of average size ∼3 nm (From Ref. [5])

1.9.2 2D-Graphene

Graphene is the first and most prominent 2D material. The exfoliation of micrometer size of graphene from bulk graphite was done successfully by Geim and Novoselov in 2004 [84]. The exploration of graphene brings new evolution in optoelectronic ap-

plications. Various research works have been done on graphene which revealed the fascinating and unique properties of graphene such as its high carrier mobility, great tensile strength, and broadband light absorption determined by the fine structure constant (α).

Graphene is an allotrope of carbon consisting of a single layer of atom arranged in two-dimensional honeycomb lattice [9]. Each atom in a graphene sheet is connected to its three nearest neighbors by a sigma-bong and contributes one electron to a conduction band that extends over the whole sheet. Graphene is an efficient conductor of electricity as well as heat due to its planar geometry. It is also 100 times stronger than the steel of the same thickness. The high carrier mobility ($>10^6$ cm^2/V-s), great tensile strength along uniform absorption of light determined by the fine structure constant for broad-spectrum make it a suitable contender for broadband optoelectronic applications. Although the weak absorption of light about 2.3% by mono-layer graphene is a concern while designing photodetectors. The low absorption of graphene can be mitigated by introducing a high absorption structure like QDs to result in a hybrid structure with highly improved optical characteristics as reported by various researchers. [23, 51, 85].

1.9.2.1 Electronic Property

Graphene is a zero bandgap semiconductor, due to no separation between conduction and valence band has been observed at the Dirac points. In the momentum space of graphene there are six Dirac points, on the edge of the Brillouin zone, divided into two non-equivalent sets of three points. At these points (K and K'), also called Dirac points, the conduction and valence band meet, thus making graphene a zero-band gap semi metal. Graphene is a single layer of sp^2-hybridize carbon atoms arranged in a two-dimensional hexagonal lattice [9]. The nearest neighbor distance of 1.42 Å between the carbon atoms is shown in Fig.1.22 (a). The nearest three atoms of carbon graphene structure are shared and formed σ bond while the remaining valence electrons formed a delocalized, out-of-plane π bond. The unbounded electron in the graphene structure results in the intriguing electronic property of graphene.

- **Band Structure:**

The band structure of graphene was firstly demonstrated by Wallace in 1947 [86] by using a tight-binding approximation. Wallace suggests that the band structure of the graphene can be obtained by dividing the honeycomb structure into two triangular sub-lattices like A and B as shown Fig.1.22 (a). Each carbon atom in sublattice A is having three neighbors atoms in sublattice B and vice versa. Fig.1.22 (b) shows the resultant band gap of graphene which shows the relationship between the energy and momentum with K and K' points in the Brillouin zone. The point K and K' in Fig.1.22 (b) are called Dirac points where the conduction and valence band meet in graphene structure and results in a gap-less semi metal. In the E-k diagram the electronic dispersion of the valence π-band and conduction π^* has been calculated by tight-binding approximation [9], here k_x and k_y are momentum vectors normalized by lattice constant (a). The red line shows the Brillouin zone and symmetry points. The zoom image in Fig.1.22 (b) shows the linear dispersion close to one of the Dirac points. Under ideal conditions i.e., at zero temperature and no doping, the fermi energy E_F of graphene exactly coincides with the Dirac points. The two sets of Dirac points i.e., K and K', corresponding to the two sub-lattices, give graphene a valley degeneracy of g_v=2. The valence and conduction band near the Dirac points where $|E|$ is less and equal to the 1 eV, can be described by a linear dispersion relation [9]

$$E(k) = \pm\hbar v_F|k| \tag{1.23}$$

where, $\hbar$ is reduced plank constant and $v_F \approx c/300 \approx 10^6$ m/s is the fermi velocity and k is wave vector. It was observed from equation 1.23 the spectrum function shows the Dirac like Hamiltonian for mass less Dirac fermions with a velocity v_F as discussed in literature [87]. The above finding attract more the study of graphene in early days.

The linear dispersion of graphene relate the density of state that is proportional to energy and given as

$$D(E) = \frac{g_s g_v}{2\pi(\hbar v_F)^2}|E| \tag{1.24}$$

where, g_s=2 is the spin degeneracy. After integrating the D(E) up to E_F the carrier

charge density in graphene is related as(From Ref. [9])

$$E_F = sgn(n)\hbar v_F \sqrt{\pi |n|} \tag{1.25}$$

So, from 1.25 the carrier density of the graphene can be continuously tune from electrons to holes by varying E_F, which is possible due to gap-less nature of graphene.

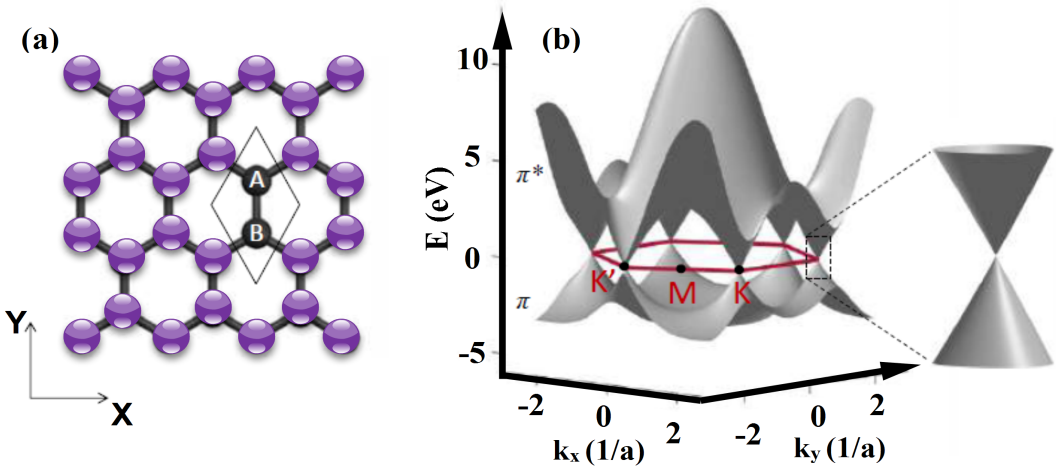

Figure 1.22: (a) The hexagonal lattice structure of graphene, (b) Band structure of graphene. (From Ref. [9])

- **Transport Property:**

The electrical conductivity of graphene increase with the number of electrons and holes, with minimum conductivity when fermi energy is at the Dirac point or neutrality point. However, due to thermal effects and local vibrations in fermi levels, there always exists a charge carrier density and therefore the conductivity of graphene never vanished completely. The popular way used to modulate the carrier density in layered materials or low dimensional materials is by applying a potential difference between the layered materials and a metallic gate separated by an insulator. The electrostatic force, also called the field-effect, that appears due to potentials differences is often used to study the transport properties of graphene [88].

For the diffusive regime, the carrier charge density (ρ) of graphene is related to the conductivity σ, and the mobility (μ), by the relation σ=ρ μ. Due to the massless nature

of carriers as well as low scattering rate with intrinsic phonons, graphene shows ultra-high mobility of the order of 10^5 cm^2/V-s at room temperature. The reported mobility of graphene is found to be far better than that of conventional semiconductor materials. The quality of the graphene could be easily determined by measuring the mobility of the graphene. The synthesis of good quality graphene is possible by employing a much-sophisticated synthesis technique like CVD [51].

The charge transport in the graphene is suffered from substrate scattering effects as well as with contaminants such as water and oxygen molecules. To improve the transportation of carriers the electrical measurement must be carried out at vacuum or under the protection of graphene surface by coating with materials like SiN, PMMA, h-BN. Protecting graphene with various substrate also improve the scattering effect in graphene and enhances the mobility of graphene. For example, the mobility of graphene has been reported maximum of 1,40,000 cm^2/V-s when encapsulated between two layers of h-BN [89].

1.9.2.2 Optical Property

The zero bandgap nature of graphene facilitates it as a 2D material with a broad absorption spectrum. The unique bandgap of graphene makes it special optoelectronic material having distinct optical properties and various types of light-matter interactions [90, 91]. The intrinsic optical absorption, by 2D layer materials including graphene, is given by the real part of their optical conductivity σ and related as per the literature [87]

$$A_{abs} = \frac{Real[\sigma]}{\epsilon_0 c} \tag{1.26}$$

where c is the speed of light and ϵ_0 is the vacuum permittivity. The optical conductivity of graphene is govern by two processes named interband and intraband optical transition as shown in Fig.1.23 (a) [87]. The black dotted line in the figure shows the uniform absorption of graphene for broad photon energy. In the inset of Fig 1.23 (a), Dirac cones showing the interband transition process allowed at $h\nu > 2E_F$, but forbidden (red cross) at $h\nu < 2E_F$ due to Pauli blocking, is given. In this regime, only

intraband transitions (curved arrows) are allowed. The happening of both interband and intraband transitions in graphene will depend on the fermi energy of graphene E_F and photon energy ($E_{pho} = h\nu$). When $2E_F > h\nu$, only intraband transitions are allowed since interband transitions are prohibited by Pauli blocking. For the realistic doping level, E_F ranges from 0.1 to 0.3 eV which corresponds to energy levels of mid to near infrared regions. For this region, the intraband absorption is due to free carrier response and can be described by the Drude model, which takes into account the scattering time of the free carriers [92, 93].

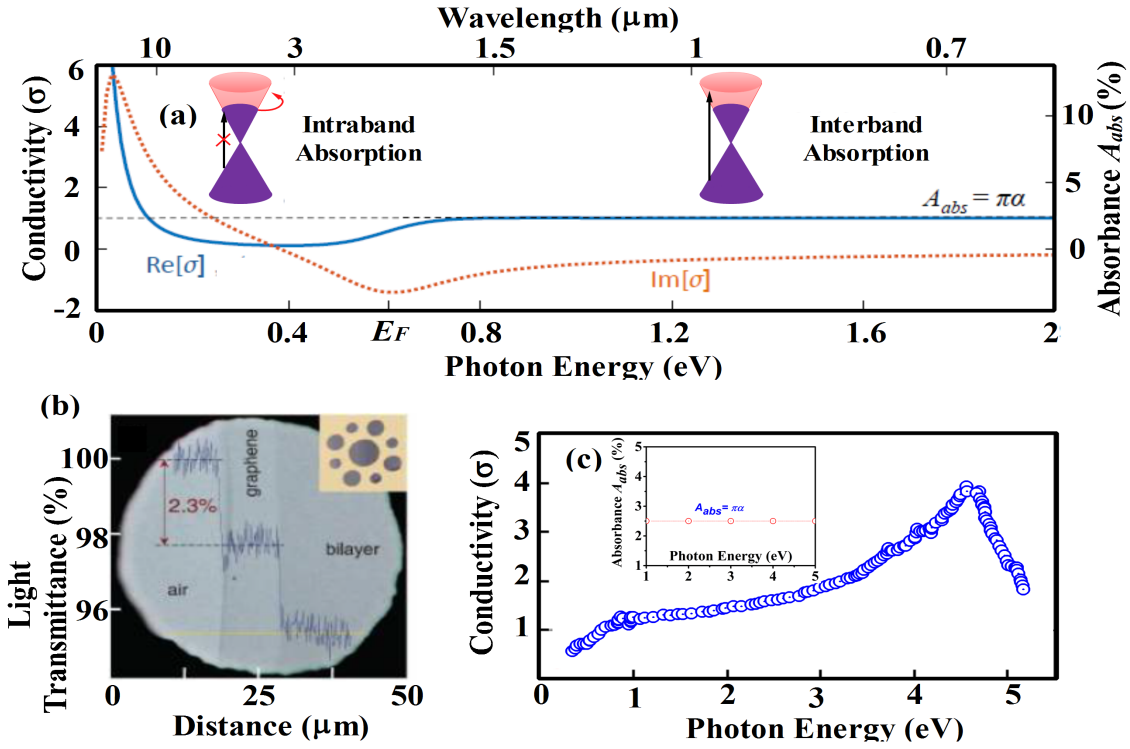

Figure 1.23: (a) Optical absorption of graphene along with its conductivity, (b) Image of an aperture partially covered by graphene and bi-layer graphene, (c) Experimentally calculated optical conductivity (From Ref. [9])

For the case of $2E_F < h\nu$, an interband transition is no longer forbidden and they dominate the optical response. It was noted that in the linear dispersion region of graphene the interband absorption does not depend on photon energy and not even any material parameters. The absorption coefficient of the graphene for this transition is defined by the universal constant given by; $A_{abs} \approx 2.3\%$ (Fig.1.23 (b,c)) where, $\alpha = {\epsilon_0}^2/4\pi\epsilon_0\hbar c$ is fine structure constant [94]. Due to the ultra-thin nature of 2D

materials, the absorption of these materials depends on the mounting substrate also due to multiple light reflections and interference. In the simplest case of a 2D layer on an infinitely thick substrate, the actual optical absorption is $4A_{abs}/(1+n)^2$, where n is the refractive index of the substrate [9]. The uniform absorption of graphene for broad-spectrum along with ultra-high carrier mobility motivated us to explore this material along with some QDs to results in an efficient and fast hybrid photodetectors. The absorption of graphene about 2.3% raises an important question when this material is used as a broad absorption material in photodetection structures. It was noted that the single atomic layer of graphene absorbs 2.3% of light is equivalent to 50 atomic layers of Si which is still very much efficient. For further enhancing the optical performance of graphene-based devices the integration of strong absorption structures like QDs, nanosheets, nanorods, etc., has been fancy used these days [23]. Therefore, in this thesis, we have studied the hybrid structures of 2D layer materials with 0D nanostructures to improve the optical response under broad light illumination.

1.9.3 TMDs: 2D-SnS_2

Zero bandgap property of graphene with poor optical absorption over a wide range of spectrum have initiated the exploration of other layered materials with better absorption properties. Transition metal dichalcogenides (TMDs) are the new class of layered materials with good absorption and sufficient tunable band gap for wide range of optoelectronic applications [95]. TMDs can be simply expressed by the formula MX_2, where M is transition metal i.e., Mo, W, Sn, and X is a chalcogen i.e., (S, Se) [96]. MoS_2 and WS_2 are widely explored TMDs materials for visible range photodetection application due to their suitable bandgap and also the strong light absorption in comparison to graphene. Similarly, $MoSe_2$ and WSe_2 have been explored for NIR regions [95]. The optoelectronic properties of mono and few-layered TMDs have been studied in recent years [97] to conclude that the optical properties like the bandgap of these materials can be easily tuned by changing the number of layers. The indirect to direct band transitions have been reported in these materials, while changing from bulk to nano-layered form e.g. the bulk form of MoS_2 shows indirect bandgap while few lay-

ers of MoS_2 shows direct band nature [98]. In conclusion, under the monolayer limits, TMDs possess a direct bandgap in the range of 1–2 eV and prove their potentiality as a new class of layered materials for many types of applications [99, 100]. Apart from the strong light-matter interaction of TMDs materials the low mobility in the range (1-100 cm^2/V-s at room temperature) and the small bandgap tunability limits these TMDs (MoS_2, WS_2, $MoSe_2$ and WSe_2) in visible and NIR spectrum detection. The various 2D materials and their corresponding detection range are shown in Fig.1.24 [101]. The detection range limitations of other TMDs motivated the researchers to explore a less known TMD layered materials called Tin Di-sulfide (SnS_2). The focus of this thesis is to explore 2D-materials (graphene and SnS_2) and their hybrid structures with the 0D (CTS QDs) material. In the next subsection the discussion of the opto-electronic properties of layered material 2D-SnS_2 have been given. In comparison to other TMDs materials, 2D-SnS_2 offers high stability, high mobility, large bandgap tunability and non-toxicity [102, 103].

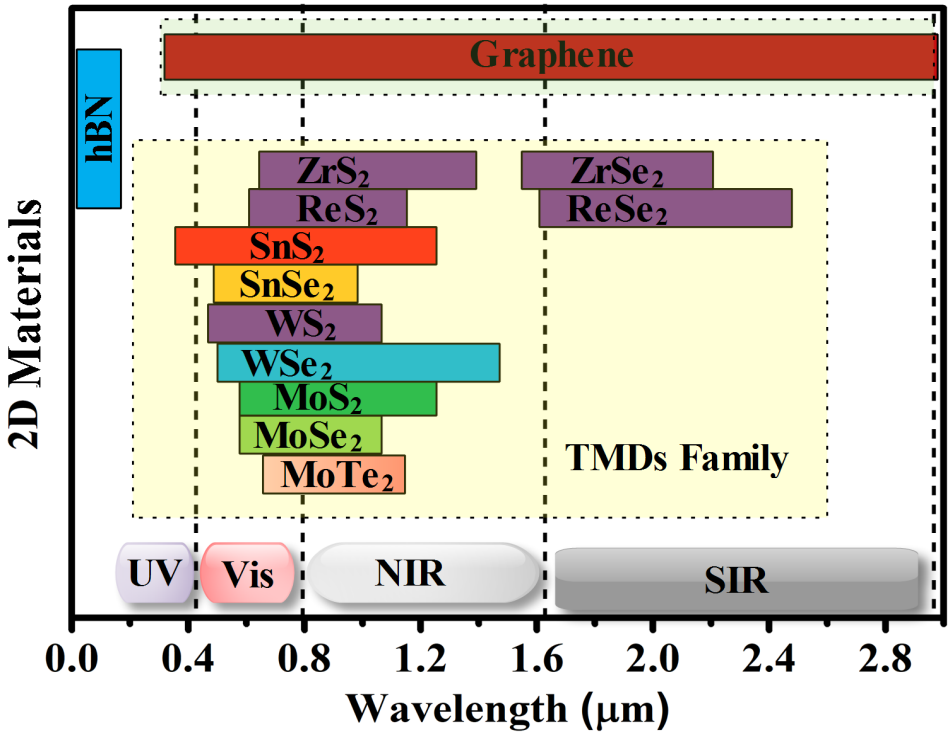

Figure 1.24: 2D materials and their corresponding detection ranges

1.9.3.1 Electronic Property

SnS_2, a layered n-type material, possess similar kind of atomic structure like other TMDs such as MoS_2, WS_2, $MoSe_2$, etc. [95] In the atomic structure Sn atoms are connected with two S atoms and form three atom-thick layer material as shown in Fig.1.25 (a). SnS_2 offers high stability and non-toxicity in comparison to other TMDs which make it a suitable contender for optical application [104]. In past, there are very few reports on SnS_2 based photodetectors while it has been widely used in the lithium-ion batteries, gas sensing, and biomedical applications [104].. The bandgap of SnS_2 is mainly reported in the range of visible region and can be tuned upto in UV and NIR region. Yourong-Tao *et al.,* [105] has synthesized nanosheets of SnS_2 having a broad range of absorption from UV to NIR. On the other hand, the other TMDs like MoS_2, WS_2, $MoSe_2$ are having their detection corresponding to 1 to 2 eV [95] therefore, find application partly in visible or NIR spectrum. The opto-electronic properties of layered SnS_2 have been summarized in Table-1.4.

Table 1.4: Some Typical Opto-electronic Properties of SnS_2

Parameters	**Values**
Energy Gap and Type	∼2 to ∼3 eV, n-Type [106]
Absorption Coefficient	10^5–10^6 [106, 107]
Density	4.5 g/cm^3 [108]
Crystal Structure	Hexagonal [10]
Carrier Concentration	10^{13} to 10^{17} cm^{-3}[109]
Melting Point	600^0C
Lattice Constant	a = b = 0.364 nm, c = 0.589 nm and $\alpha = \beta = 90^o$, $\gamma = 120^o$ [10]
Electron mobility	18.3–230 cm^2/V-s [106]
Thermal Conductivity	0.78 W/mK [106]
Stable Phase at 300 K	2H-SnS_2 [108]
Electric Conductivity	10^{-4} to 10^{-7} S/cm [106]

- **Crystal and Band Structure:**

SnS_2 has a layered CdI_2-type structure in which the tin atoms are located between two hexagonal close-packed sulfur slabs to form a three-atom sandwich structure

(S–Sn–S triple layer) [11] as shown in Fig.1.25 (a). In Fig.1.25 (a) Sn and S are bound via a strong covalent force within each triple layer. Each triplet layer having bounded Sn and S atoms is separated by other triplets S-Sn-S atomic layer by weak Van der Waals force, making this material easily integrable with other TMDs layered materials [10]. SnS_2 can be exfoliated to form two-dimensional (2D) crystals because of its special structure [10].

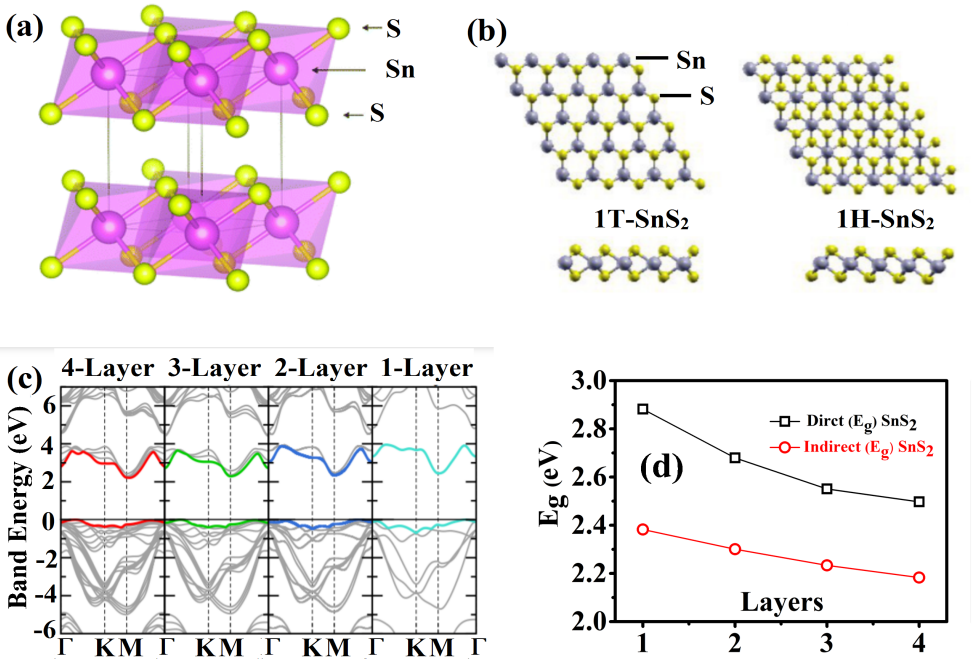

Figure 1.25: (a) Layered atomic structure of SnS_2, (b) Top and side view of mono layer 1H-SnS_2, and 1T-SnS_2 (c),(d) Band gap variation in few layer SnS_2 (From Ref. [10, 11])

In a study the authors [10], have investigated the phase structure of SnS_2 along with bandgap dependency on the number of layers of SnS_2 as shown in Fig.1.25. The mono-layer SnS_2 shows two phases named as 1H-SnS_2 and 1T-SnS_2 as predicted by DFT. The unit cell of both phases is a hexagonal prism. The atomic structure of both phase structures is shown in Fig.1.25 (b). Both phase structures are having hexagonal prism but the difference is found in the way of sandwiching the Sn atoms. The 1H phase is of trigonal prismatic style such that S atoms occupy the equivalent position with space group of $P\bar{6}m2$ as shown in Fig 1.25 (b). On the other hand in the 1T phase, the S layer is closed packed as shown in Fig.1.25 (b) and belongs to $P\bar{3}m2$ space group. The

lattice parameters for both structures are predicted by the researcher in their study and show good agreement with experimentally calculated data. The calculated lattice constants a_o of 3.62 Å and 3.70 Å were obtained for 1H and 1T phases, respectively. The bond length between S-Sn is reported to be 2.64 Å and 2.60 Å for 1H and 1T phases, respectively. From literature, it was known that IT-SnS_2 is the most energetically favorable phase [10].

Apart from the above-discussed phase of SnS_2, there are some other phases 2H ($P\bar{3}m1$), 4H ($P6_3mc$) and 18R ($R\bar{3}m$), reported by the various researchers, dependent on the growth conditions [108]. There are various growth techniques explored for SnS_2 nanostructures like CVD, molecular beam epitaxy, vapor epitaxy, and solution-based synthesis [11]. Depending on growth condition and growth techniques SnS_2 can appear in several poly-types including 2H, 4H, and 18R [11]. In this thesis work, we have achieved SnS_2 having 2H phase (most stable phase)[108] by employing a low-cost solution-based technique.

Fig.1.25 (c) shows the layer dependent electronic band structure of SnS_2 as reported in literature [11]. Compared to MoS_2, SnS_2 shows the indirect band gap nature even at its single-layer form. The change in band structure of SnS_2 by changing the number of layers has been studied in detail in literature [11]. Fig.1.25 (d) shows the layer dependent indirect and direct band gap of SnS_2 nanostructures. From the detailed band gap study of SnS_2 in literature [11] close to the Fermi energy, the band structure of mono-layer TMDs (including SnS_2) can be represented by two sets of degenerate conduction and valence bands around the K and K' points, with parabolic dispersion relations [9]:

$$E(k) = \pm \frac{\hbar^2 |k|^2}{2m^*} \tag{1.27}$$

where m^* is the effective electron or hole mass. For TMDs materials m^* lies between 0.4 m_0 to 0.6 m_0, where m_0 is the electron rest mass. In equation (1.27), k is the wave vector measured from the K or K' point. Interestingly, this resembles the spectrum of a 2D Dirac Hamiltonian for massive Dirac fermions, which also describe carriers in gaped graphene [110].

- **Transport Property:**

The carrier transport in 2D-SnS_2 has been described in lines of carrier transport in TMDs in general. The dominant factors effecting the carrier movement in 2D-SnS_2 are carrier mobility limited by the carriers scattering, edge effects on mobility, short channel effects and ballistic transport carrier mobility and carrier scattering effects, carrier transport and the scattering limited mobility edge effects, and short channel effects and ballistic transport [111, 108, 111]. The carrier transport has been affected by the number of layers of 2D-SnS_2, the temperature of operation of the device, and the type of substrate chosen to mount the device [108, 111]. The 2D nanomaterials do exhibit for superior carrier transport compared to the bulk counterpart.

1.9.3.2 Optical Property

Due to the existence of bandgap, TMDs have optical properties radically different than those of graphene. While they are transparent to long wavelengths, TMDs display high optical absorption and emission in the near-infrared and visible spectral region. These strong light-matter interactions are a consequence of the enhanced carrier-carrier interactions, which give rise to prominent excitonic effects [112]. These strong excitonic effects have a large impact on the absorption and emission spectrum of TMDs. This optical transition, therefore, governs the absorption in TMDs in the near-infrared and visible region, regardless of their layer numbers [113].

SnS_2 is probably the best material explored among TMDs due to its better chemical stability, non-toxicity, environment friendliness nature, and band gap tunability over some UV, UV-visible, UV-visible-NIR band spectrum [114, 106]. The SnS_2 nanostructures of various morphology i.e., nanosheets, nanoflowers, nanowires, QDs, etc., and synthesized by various methods including CVD [107, 96], hydrothermal [115], ultrasonic chemical method (UCM) [116], anodization [117] and liquid phase exfoliation (LPE) [118] is shown in Fig.1.26. The good optical absorption of SnS_2 as well as the broad range i.e., UV-Vis-NIR tuning capability results this materials a strong contender for broadband photodetection [116, 96]. Apart from the strong absorption coefficient about $\sim 10^5$ cm^{-1} [107], the SnS_2 possess the highest mobility of 230 cm^2/V-s [119]

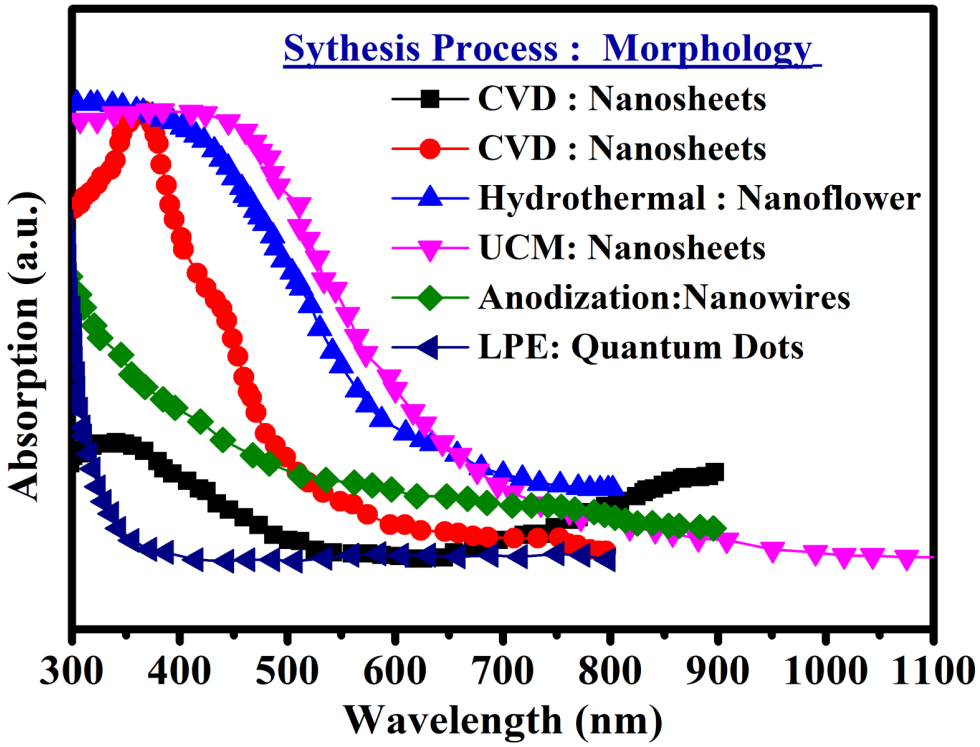

Figure 1.26: Optical absorption of SnS_2 nanostructures synthesized by different techniques

compared to other TMDs having the room temperature mobility in the range of 1-100 cm^2/V-s. The broad range absorption as well as the good mobility of SnS_2 along with simple one-pot synthesis techniques are the key motivation to explore this material in this thesis. This not only reduces the overall fabrication cost but also remove the requirement of additional active materials and reduces fabrication complexity for broadband applications. The broadband photodetection of SnS_2 nanostructures with superior optical characteristics has been studied by various researchers in their reports [107, 105, 118, 120].

1.10 Literature Review

Broadband photodetector based on 0D, 2D and the hybrid structures are having a wide range of applications. A continued effort is observed in literature toward improving the performance of the broadband photodetectors derived from any such materials. After

the discussion on the optoelectronic properties of 0D-CTS QDs, 2D-graphene and 2D-SnS_2 in the introduction this section discusses some state of the art structures based on these materials and their hybrid for broadband photodetection.

1.10.1 Some State-of-Art work on 0D, 2D and 2D/0D Nanostructures for Broadband Photodetection

The 0D quantum dots are widely used in broadband photodetection applications due to their size-dependent bandgap tuning property and also they possess a high absorption coefficient in comparison to other low dimensional materials due to their large surface-to-volume ratio. On the other hand, 2D materials with ultra-high mobility like graphene and high absorption coefficient of some 2D-TMDs like SnS_2 have been explored in broadband photodetection applications [121, 103]. The hybrid structure of these 2D materials has been studied in the current thesis with a new and less explored vis-NIR active material i.e., CTS. The CTS material has proved its potentiality in broadband photodetection due to its low toxicity, earth-abundant, high absorption, and large bandgap tuning nature in comparison to other materials like PbS, PbSe, HgTe, CdTe, etc., used for the same detection range [64].

So, in this section, we will discuss study of some QDs structures for broadband photodetection applications and compare their performance with the less explored CTS QDs structures. In the latter half of this section, we will study some simple and 2D/0D hybrid nanostructures for broadband photodetection and conclude our discussion by exploring 2D graphene and 2D-SnS_2 over other layered 2D materials due to their ultra-high mobility, large tuning range, non-toxicity, and higher stability [102, 103].

1.10.1.1 Conventional Quantum Dots (QDs) for Broadband Photodetection

The realization of broadband photodetection through colloidal Quantum dots structures is more demanding these days due to their quantum size effect [122, 123, 124]. The quantum size effects in the nanostructures give a variety of unique phenomenon such as size tunability, multi-exciton processes, [125, 126] high surface to volume ratio, and

strong matter to light interaction. Apart from the quantum dots effects, most colloidal QDs nanostructures are synthesized by low-temperature one-pot solve/hydrothermal techniques which reduces the overall fabrication cost of colloidal QDs based devices.

The popular materials mostly used for Vis-NIR broadband detection such as PbS, PbSe, CdTe, HgTe, etc., [127, 128, 129] are seriously sufferers from wide limitations. In the context of NIR photodetection through simple and hybrid photo-conduction structure Andrea *et al.,* Keke *et al.,* and Xingtian *et al.,* [130, 131, 132] has discussed and summarized the optical performance for NIR region due to large bandgap tunability of PbS QDs. The high toxicity of Pb with the inefficient carrier transfer due to long ligands decoration limits their optical response and degrade their performance. In the continuation of broadband realization with improved performance of PbS QDs structures, Longfei *et al.,* and Haodong *et al.,* [133, 134] has realized PbS QDs photodetector structure by exploring new ligand exchange methods in QDs structures at the cost of involving complexity in the synthesis of QDs. The hybrid structure of PbS QDs has been explored by the various researchers [135, 136, 137] to improve the performance of PbS QDs structures at the cost of enhancing the overall cost and detection volume of these hybrid structures. Further, PbSe QDs having almost similar optoelectronic properties as PbS QDs [138]. Gebril *et al.* [139] has realized a hybrid PbSe QDs structures with high mobility materials like graphene for broad NIR photodetection with enhancing optical performance. Tom *et al.,* [140] has also reviewed the performance of some hybrid structures of PbSe QDs over PbS QDs structure and their comparative study over broad NIR regions. Instead of having better performance, the highly toxic nature of Pb elements limits their applications including in biological fields.

In the substitution of PbS and PbSe materials based QDs photodetectors for NIR regions the other QDs structure materials based on HgTe for the NIR region have been explored [141, 142] due to their broad range absorption cover almost all NIR regions. The low-temperature operation of HgTe QDs structures [143, 144] suffers from the temperature-dependent optical characteristics. The poor temperature stability of HgTe QDs devices [145] require a large cooling system in ambient condition [143] and increase the overall detection cost. Further, the synthesized HgTe CQDs have poor

surface stability, which leads to two problems. First, HgTe CQDs easily aggregate and crash from solution over time; second, to stabilize the colloid, one has to use strong ligands such as thiol [146], which generally modified the HgTe QDs surface. The poor surface stability of these QDs structure has been controlled by the proper doping in these QDs structures as discussed by Shen *et al.,* in their study [146] which increases the synthesis complexity and overall fabrication cost for these materials based broadband photodetector and also offers the toxicity due to Chang-Ching *et al.,* Xilan *et al.,* and Lei *et al.,* has further studied a limited visible band CdTe QDs based simplest and hybrid detectors [147, 148, 149] with improved optical performance but again the high toxicity of Cd limited their applications in biomedical applications while the rarity of Te also the major drawback in these detectors. The toxicity of CdTe QDs structure has been studied by Aiwu *et al.,* [150] and suggest a silica coating over it to improve surface toxicity as well as to improve the surface property of CdTe QDs at the cost of complex synthesis along with extra material integration. The rarity of Te is also an issue [151] for such types of detectors. Further, the limited bandgap tunability only for vis or NIR and toxicity of PbS, PbSe, and HgTe leads to the limited applications in optoelectronic devices [63, 64].

These major drawbacks of these conventional QDs structures lead the researcher to look out for some other materials with non-toxic, earth-abundant, high absorption, large bandgap tunability, and environment-friendly properties for broadband photodetection applications.

1.10.1.2 Cu_2SnS_3 Nanostructures and their QDs Based Broadband Photodetection

The limitation of conventional broadband vis/NIR QDs based photodetection structure has motivated the researchers to look out for a substitution of this materials. Recently, Cu_2SnS_3 (CTS) a highly stable, nontoxic, earth abundant [152, 153, 154] p-type semiconductor materials having high absorption coefficient 10^4 cm^{-1} is being investigated for photodetectors [5]. The CTS QDs have wide range of photodetection (Vis-NIR, 1.68–0.67 eV) [7] due to their large band gap tunability Over other QDs structure used

for this detection ranges. The strong visible-to-NIR range detection property of CTS materials has been widely used in photovoltaic applications. V. R. M. Reddy *et al.,* T. Srinivasa *et al.,* and Jianmin *et al.,* [3, 70, 155] has reported the low cost solvothermal synthesis of CTS nanomaterials and studied their photovoltaic applications and results a good external quantum efficiency. V. R. M. Reddy *et al.,* has also studied the phase stability of Cu-Sn-S structure family over other combination. In their study Cu_2SnS_3 possess the wide range of structure stability, good hole-mobility, high conductivity and also shows the optical efficiency over Vis-NIR spectrum ranging in 10%-60%. The favourable property for photo-voltaic application of CTS materials and their nano structure motivated the researcher to explore these materials for photodetection applications. In the beginning, S. Dias *et al.,* [63] has synthesize a Cu_2SnS_3 thin film by a low cost solvothermal technique and realize a vis-NIR photo-conduction structure with maximum external quantum efficiency of $\sim$10% over soda lime glass (SLG). In the next phase, T. S. Reddy, *et al.,* [156] has studied the varying thickness dependent analysis of CTS thin film by taking photo-conduction structure and also studied the crystalline structure of CTS by changing the temperature confirming the Vis-NIR photodetection with improved quantum efficiency but this leads large dark current which degrades the detectivity of this structure. Sandra Dias *et al.,* [157] have studied the effect of illumination intensity of photon over CTS nanostructure and reports the improvement in the optical performance including responsivity, detectivity and EQE for a high quality flower and sphere shaped CTS nanostructures. In the context of improvement in the performance of CTS based structure for broadband illumination, Sandra Dias *et al.,* [64] has further investigated an organic and inorganic hybrid structure of CTS. The various structures of varying concentration of CTS nanostructure in the organic polymer have been studied and the performance of these structure were measured over NIR regions. The resultant hybrid structure shows the responsivity, sensitivity, EQE and detectivity 211.5 mA/W, 3.6, 32.8% and 8.7×10^9 Jones, respectively at the cost of fabrication complexity and also low detection bandwidth in NIR. In the continuation of hybrid structure of CTS materials S. Dias *et al.,* [7] investigated first time the QDs structure of CTS and then pattern it over ITO substrate and realize a hybrid structure.

They report the variation of CTS QDs size by varying the reaction time and also the temperature. A QDs of size range of 2.7 nm to 3.6 nm have been synthesized and their band gap corresponding to their size variation were measured. The resultant structure discussed in this study has shown sufficient improvement in the optical performance of structure due to QDs structure of CTS over other nanostructures of CTS due to its higher surface to volume ratio. The structure shows high values of responsivity, external quantum efficiency and specific detectivity 1.76 A/W, 272.53% and 2.79×10^{11} Jones, respectively at small 0.5 V applied bias at the cost of fabrication complexity. In the continuation of this [5] report a solvothermal synthesis of CTS QDs with size of $\sim$3 nm has been investigated for the performance in the hybrid structure for NIR illumination. Apart from the optoelectronic performance of CTS based devices as discussed here it was noticed that their optical performance are still very low for advance optoelectronic applications in the range of Vis-NIR detection.

The performance of these structure has been improved at good extent by employing hybrid structure like in [5, 7] with suitable substrate but improvement are still very small. The improvement in the CTS QDs structure could have been performed at good extent by integrating them with ultrahigh mobility materials like 2D-graphene and some other class of 2D materials like TMDs due to their high absorption coefficient for broadband spectrum.

1.10.1.3 2D-Graphene and their Hybrid (2D/0D) Structures for Broadband Photodetection

Two-dimensional layered materials bring a new revolution in the field of optoelectronics due to their atomic thick structure over conventional materials. After the first isolation of graphene by Andre Geim and Konstantin Novoselov in 2004 [158] from bulk graphite enormous interest for these materials was triggered. The weak inter-layer interaction for these materials makes it suitable for them to easily exfoliated individual layers from the bulk. The easier integration due to weak Van der Waals forces and ultrahigh mobility of graphene due to in-plane carriers motion [159] result in their wide range of applications in fast and broadband photodetection. Apart from high favorable

optoelectronic properties, graphene possess high tensile strength and super-thermal conductivity [159].

In the context of broadband photodetection Fengnian *et al.,* [160] group in 2009 has fabricated and characterized the simplest graphene-based photoconductor structure. The research group in that study [160] report, ultra high speed in the structure but their responsivity is very poor about 0.5 mA/W at high applied voltage. Similarly, in 2010, Thomas *et al.,* [161] has also reported a graphene-based ultra-fast broadband photodetector while their responsivity is limited up to 6.1 mA/W. Similarly, Lemme, Max C. Max Lemme *et al.,* M. Nathaniel *et al.,* and Marcus Freitag *et al.,* [162, 163, 164] have also reported the graphene p-n junction based structure but they report the responsivity of these structure in the range of few mA/W and also leads fabrication complexity.

The smaller photoresponsivity of these structures results from the low absorption of graphene about 2.3% for broadband illumination. Due to the zero bandgap nature of graphene which turns it into a semi-metal material with ultrahigh mobility of the order of 10^5 cm^2/V-s results in a high-speed material with very poor optical characteristics i.e., responsivity, detectivity, EQE, etc. The best possible way to create a bandgap opening is by disturbing the symmetry in the atomic structure of graphene through applying high electrostatic force, appropriate doping, and the integration with various substrates as reported by Xiong *et al.,* [165]. The above integration technique requires high fabrication complexity and some sophisticated techniques like molecular beam epitaxy (MBE), lithography, etc., therefore, enhance total fabrication cost.

Various studies have been carried out to improve the responsivity of the graphene-based structures with other materials as discussed in literature[166, 167]. In 2012, Gerasimos *et al.,* [168] has fabricated and characterized a hybrid structure of graphene with QDs structure with huge responsivity about 10^7 A/W and also the speed in ms at the cost of toxicity of PbS QDs material. The obtained optoelectronic parameters for the 2D/0D structure for broadband detection bring a new idea to enhance the performance of graphene detectors by integrating it with high absorption nanostructures called QDs due to their higher surface to volume ratio. A large number of studies have

been carried out to realize graphene-based hybrid structure with OD-QDs. Leyla *et al.,* [169] has reported a broadband structure based on Graphene/0D-MoS_2 with an ultra-high response but observe the low external quantum efficiency of 20% due to small bandgap tunability of MoS_2-QDs in visible range which hampers the broadband performance. Recently, V. K. Singh *et al.,* [51] in 2019, reports a large-area CVD grown graphene and study its photodetection performance for broadband illumination. The ultra-high responsivity has been reported here in UV regions due to high absorption of QDs structure while the responsivity degrades for visible and NIR band. Similarly, Nguétchuissi *et al.,* [170] has reported the hybrid structure of graphene with HgTe QDs with broadband NIR detector, but the toxicity and stability of HgTe in ambient conditions force the researcher to look for other QDs structures. The review study by Xuewan *et al.,* [171] demonstrated the various two-dimensional materials and their QDs structure with graphene and their optoelectronic performance over a broad spectrum.

From the above state of art discussion, it is observed that the graphene is good for the transport layer function to realize an ultra-fast photodetector but the zero bandgap nature of this material and very poor absorption in UV-Vis-NIR limit their responsivity in few mA/W. The poor responsivity of graphene-based structure has been improved sufficiently by integrating it with high absorption nanostructures called 0D QDs. The broad range and high absorption QDs structures, with no toxicity and high stability could be the best choice QDs to design an efficient broadband photodetector.

1.10.1.4 2D-Transition Metal Dichalcogenides (MX_2; M = Mo, W, Sn etc., & X = S, Se) Based Broadband Photodetection

After several years of intensive research on graphene, the attention gradually shifted towards other 2D materials, mainly hexagonal boron nitrite and transition metal dichalcogenides (TMDs). Hexagonal boron nitride is a transparent insulator. While TMDs are layered compounds with general formula MX_2 where M is a metal from group IV, V, or VI of the transition metals and X is a chalcogen atom (group-VI, e.g., S, Se or Te) [172, 22, 96]. TMDs materials offer high absorption in comparison to graphene and are treated as a suitable contender for broadband photodetection. Along with higher

absorption, TMDs also shows a variety of electronic transport phase: metallic, superconducting, charge density wave and semiconducting. TMDs also exhibit a crossover from indirect to direct bandgap in the monolayer limit. The photodetection application of TMDs materials like MoS_2, WS_2, WSe_2, and $MoSe_2$ are generally limited to the visible to NIR spectrum due to their bandgap tunability between 1–2 eV [99].

The broadband detection structure based on TMDs mostly falls in visible and NIR bands due to their bandgap engineering [99]. The photodetection structure with TMDs has been widely explored these days due to their favorable optoelectronic properties. Yin *et al.,* [173] first report photodetectors based on single-layer MoS_2 and report the responsivity of about 7.5 mA/W. The structure broadband response is further decreased due to no photon absorption by MoS_2 layer due to their limited visible band tendency and also the structure having the complexity of single layer synthesis of MoS_2. In continuation of MoS_2, based visible band detectors Zhang *et al.,* [174] has reported an improved responsivity by synthesizing a single layer of MoS_2 by CVD and exfoliation technique by improving the surface to volume ratio of structure. The bandgap tuning of MoS_2 has been further studied to extend the detection range by Sung Hee *et al.,* [175] and Woong Choi *et al.,* [176] and also leads to larger absorption due to an increase in thickness of MoS_2 and reported the responsivity similar to single layer photodetectors.

Further, $MoSe_2$ based broadband detectors grown by the CVD technique have been analyzed by Yung Huang *et al.,* [177] and Jing Xia *et al.,* [178]. The responsivity of CVD grown $MoSe_2$ detectors are found between 0.26 mA/W and 13 mA/W for Vis-NIR detection [177, 178]. The optical characteristics of the structures in the above studies show good values but at the cast of high toxicity and instability of $MoSe_2$. Further, in literature [179, 180, 181, 26] a review analysis on WS_2 and WSe_2 and their hybrid structures has been carried out. based detectors for limited band (UV-Vis/Vis-NIR) detection. The given studies on resultant complex hybrid structures of WS_2 and WSe_2 shows limited band (UV-Vis/Vis-NIR) photon detection along with high fabrication complexity.

From the above discussion, it was concluded that the limited bandgap nature, toxicity, instability of popular TMDs (MoS_2, $MoSe_2$ etc.) with small absorption coefficient

leads the researcher to look out for some other materials with high stability and non-toxicity and also having high absorption coefficient.

1.10.1.5 2D-SnS_2 and their Hybrid (2D/0D) Structures for Broadband Photodetection

As an important member of TMDs, tin disulfide (SnS_2) has sought attention recently due to its large bandgap tunability, high mobility, and high absorption coefficient, non-toxic and highly stable structure over other TMDs [182]. Tin disulfide (SnS_2) is a semiconductor material offers best electron mobility of 230 cm^2/V-s [119] and high absorption coefficient 10^4 cm^{-1} [103] in comparison to other TMDs materials like MoS_2, WS_2 etc. It is noteworthy that SnS_2 is low-cost and nontoxic, and its component elements are readily available. Over several years, a variety of SnS_2 micro-/nanostructures have been synthesized such as hierarchical microspheres [183] nanoplates, nanorods, nanowires, nanobelts, nanosheets, nanoflowers, nanotubes, and hollow spheres, and they have been extensively applied to solar cells, photocatalysts, lithium-ion batteries, and field-effect transistors [182, 183]. However, there are very few reports available on SnS_2-based photodetectors. The low exploration of SnS_2 materials along with large tuning range [183] as well as the high stability and non-toxic nature motivated the researcher to look out the application of SnS_2 for broadband photodetection. SnS_2 and their hybrid structure with other active materials are widely used for broadband photodetection due to their favorable properties [96]. Yourngo *et al.,* [105] has studied the broadband (UV-vis-NIR) absorption of SnS_2 nanostructure and realized a photoconductor structure. The responsivity of the structure was noticed very poor for the broad spectrum which results from the defects present in the nanosheets resulting from mechanical exfoliation. Later on by Xiansheng *et al.,* and Guoxiong *et al.,* [184, 185] grown a high-quality SnS_2 nanoflakes with CVD technique over SiO_2 substrate. The thickness-dependent study of SnS_2 has been carried out in the structure with high responsivity and time response. The discussed photodetection structure for broadband photodetection only by SnS_2 as an active material involves the CVD technique and improves the overall cost of photodetection structure. In the hybrid structure of SnS_2

with QDs a high absorption materials various structure has been studied to realize a broadband UV-vis-NIR photodetector. Yun Huang *et al.,* [96] has studied a CVD synthesized SnS_2 hybrid structure with a CIS QDs with high responsivity for the visible spectrum. Similarly, Liang *et al.,* [128] has studied a hybrid SnS_2 nanosheets/PbS QDs structure for broadband (300 nm-1000 nm) detection. The structure shows the ultra-high responsivity of the order of 10^5 A/W for broad-spectrum due to broad absorption of PbS in Vis-NIR while SnS_2 work as absorption materials for UV illumination. The reported responsivity is the best among the other SnS_2 based complex hybrid structures [186, 187, 188, 189] but the toxicity of PbS limited its applications. Therefore, look out for some alternate nontoxic QDs materials is going on.

1.10.2 Major Observation from Literature Review

The major observation from the literature survey can be summarized as follows.

- Among various nanostructures, QDs structure offers a high surface to volume ratio and large bandgap tunability by varying their particle sizes [190]. As compared to widely used Vis/Vis-NIR active QDs structures like PbS, PbSe, HdTe, and CdTe, CTS QDs offers, high absorption coefficient, environment-friendly, nontoxic nature, high phase stability, and is earth-abundant [64, 63, 7].

- There is a need for simple and cost effective synthesis method to reduce the overall cost of the fabrication of photodetectors. The simplest and cost effective one-pot solvothermal technique are available to be used to synthesize both of the active materials i.e., CTS QDs and 2D-SnS_2 nanoflakes structures used in this thesis.

- The simplest lateral type photoconductor structures can be used to realize a CTS QDs based photoconductor in comparison to previous CTS-based structures not utilizing QDs structure [64, 156, 157]. The optical performance CTS QDs based structure can be improved in terms of low detection volume, simplest device structure, broad detection range, and nontoxic nature in comparison to some hybrid and simplest toxic, unstable vis/NIR PbS, CdTe, and HgTe based photoconductor structures [127, 128, 129].

- The long insulating ligand used in the colloidal synthesis of QDs structure prevents the carriers to take an active part in the photocurrent [133, 128]. The poor continuity of QDs film over large area degrade the mobility of the QDs structure and could be improved at a good extent by reducing the channel spacing and multiple coating of QDs film to improve the continuity of the film over a small area.

- The poor performance of CTS nanostructures [64, 156, 157, 5] for broadband (Vis-NIR) spectrum due poor continuity as well as carriers transport of CTS films can be improved by integrating this materials with ultra-high mobility i.e $\sim 10^5$ cm^2/V-s material graphene. The integration of QDs nanostructures with high-quality CVD grown graphene will facilitate a high conducting path for the carriers generated in QDs structure under light illumination and improve the optical characteristics like responsivity, EQE, sensitivity, etc., of the hybrid 2D/0D structures [168, 51] in comparison to graphene-based broadband photodetectors not involved QDs structure [160, 161].

- The low absorption (2.3%) [191] of graphene over a large spectrum limits the operation of graphene-based photodetectors and having the responsivity in the range of few mA/W [160, 161]. The drawback of zero bandgap nature, as well as poor absorption of graphene, leads the researchers to look out for the substitution of this material by a material having high absorption coefficient, nontoxic, earth-abundant, large bandgap tunability, high stability, and good carrier mobility.

- Beyond the limitation of graphene for broadband detection a new class of low dimensional layered material called TMDs have been explored. Out of these TMDs materials some of them like MoS_2, $MoSe_2$, WS_2, WSe_2, etc., are having their bandgap tunability between 1–2 eV [100] which covers only small visible and NIR spectrum and also having low absorption which degrades and limit their performance for Vis-NIR broadband [192].

- SnS_2 a large bandgap, nontoxic, earth-abundant, and high absorption coefficient has been explored for UV-Vis-NIR photodetection [105] could be used as a po-

tential contender to consolidate the poor absorption of graphene and could realize a broadband photodetection structure over other limited bands TMDs and graphene-based structure[100, 192]. The hybrid structure of SnS_2 nanostructure with OD QDs has been further explored to enhance the performance of detection along with bandwidth extension as discussed in literature [96, 128]. Thus, the literature survey could be used to identify the gaps in 2D/0D hybrid broadband photodetection realization.

- The low-cost, non-toxic, easily synthesized one-pot technique like solvothermal could be used to realize a low-cost 2D/0D nanostructure-based broadband photodetector in comparison to other costly techniques used to synthesize 2D-SnS_2 nanostructure to reduce the overall fabrication cost of the structure.

1.11 Motivation and Problem Definition

Broadband photodetection find their various application in medical diagnosis, optical fiber communication, night-time surveillance, environment monitoring, and remote sensing etc.[26] 2D and nanomaterials have excellent properties to be useful in fabricating Broadband photodetectors. However, there are certain issues to be addressed while designing photodetector based on such materials. This thesis basically employ the hybrid of 2D/0D nanostructures to achieve efficient photodetectors operating in a broadband. The selection of the materials have been done if the basis of extensive analysis and literature review.

Cu_2SnS_3 is a low cost, p-type, earth-abundant and non-toxic element over the other materials used for same Vis/NIR photodetection like PbS, CdTe, $Hg_{(1-x)}Cd_xTe$ structure. However, the high cost of In and Te as well as the toxicity of Cd and Pb and the thermal instability of Hg in ambient conditions are issues of concern fuelling the need for the lookout for alternative materials. The CTS materials and their nanostructures offer a bandgap between 0.93-1.71 eV and also possess a high absorption coefficient of 10^4 to 10^5 cm^{-1} [64] over other quantum dots structures used for vis/NIR photodetection. The simple and low-cost synthesis of the QDs structure facilitates the large area coating and

also offers compatibility with all substrates. The large area coating-based colloidal QDs suffer from poor continuity which results in poor mobility in their structure [133]. The multilayer coating as well as reducing the channel spacing in such devices could improve the optical response of QDs structure [133]. The low conductivity of QDs structure can be further improved by involving high conducting 2D layer sheets like graphene. The hybrid structure of QDs with graphene can be purposed by utilizing the high mobility of graphene and work as a charge transporter layer for the photo carriers generated in 0D/2D hybrid structure [51, 193].

The bandwidth extension could also be possible in QDs based simplest photoconductor structures by integrating them with other 2D-materials with high absorption coefficient unlike graphene having broadband absorption of only 2.3%. 2D-SnS_2 an element of layered materials called TMDs offers high stability, non-toxic, earth-abundant, and also high absorption coefficient of the order of 10^5 cm^{-1} and offers low-cost solvothermal technique over CVD [103]. The low-cost synthesis of both nanostructures i.e., 0D and 2D reduce the overall fabrication cost and also extend the detection range due to broad absorption of both materials in their respective detection range as discussed in the literature. [96, 128]

1.12 Scope and Organization of the Thesis

The main objective of the thesis is to synthesize non-toxic CTS QDs by using low-cost solvothermal technique as a broadband photodetection material. A low-cost solvothermal synthesized CTS QDs has been used to fabricated the simplest photo-conductor structure over other complex broadband structures. The optical performance of the CTS QDs based structure for visible-NIR has been improved by integrating it with a high mobility 2D-graphene and realized a 2D/0D graphene/CTS QDs based broadband photodetector. Further, the optical parameters, as well as the bandwidth enhancement, has been carried out by employing a highly stable, low toxic 2D-SnS_2 nanostructure due to the high absorption of this material over graphene. The fabrication and characterization of SnS_2 nanoflakes/CTS QDs 2D/0D structure shows their potentiality in terms

of broadband (UV-Vis-NIR) realization and efficient optical performance compared to 2D/0D graphene/CTS QDs and stand alone 2D-SnS_2 nanaoflakes based photoconduction structures.

The remaining contents of other chapters are organized as follows

Chapter-2 discuss the low-cost solvothermal synthesis of CTS QDs. The structural characterizations of CTS QDs are done by the X-RD analysis, TEM, FE-SEM, EDX, and elemental mapping. On other hand, the absorption of the solvothermal synthesized QDs is confirmed by absorption spectra over large broadband and also the bandgap of materials using CV measurements. The simple and low-cost fabrication structure is proposed by drop-casting CTS QDs over small spaced Ag contact to realized an Ag/CTS QDs/Ag photoconductor structure. The resultant device structure offers a comparative and improved optical performance over other CTS nanostructure and also with some other QDs structures like PbS, PbSe, HgTe, etc., along with low cost, non-toxic and simplest device structure.

Chapter-3 discuss the hybrid structure of CTS QDs with a high mobility layered 2D-graphene. This chapter will discuss the hybrid structure of 2D-Graphene/CTS QDs with the improved optical performance of the device over the CTS QDs structure discussed in Chapter-2. The structural and optical characterizations of the CVD synthesized graphene are confirmed by Raman spectroscopy and also with HR-TEM analysis to insure the number of layers as well as the quality of graphene. While in the other hand the structural and optical characterizations of the hybrid structure are further confirmed by FE-SEM, TEM, absorption spectra, etc. The improved performance of the hybrid photoconductor has been studied by measuring the I-V response, current wavelength response of the structure over a large visible-NIR (650-1100 nm) spectrum.

Chapter-4 presents an efficient UV photoconductor based on SnS_2 nanoflakes. The SnS_2 nanoflakes of height distributed between 5-15 nm have been synthesized with a low-cost solvothermal technique. The high crystalline wurtzite structure with hexagonal phase geometry of SnS_2 nanoflakes has been confirmed by X-RD analysis and Raman spectroscopy. The synthesized 2D SnS_2 materials over other TMDs have been explored in this chapter due to their high stability, low toxicity, large bandgap tunability, and

also having high absorption coefficient. The optical performance of the fabricated device structure has been studied under broad light illumination. The proposed simplest photoconductor structure shows strong optical characteristics for UV light while its performance degrades toward visible-NIR regions.

Chapter-5 reports the hybrid structure based on SnS_2 nanoflakes/CTS QDs for UV-Vis-NIR photodetection. This chapter is about the improvement of the low absorption of graphene which degrades the performance of graphene-based structures in terms of their sensitivity as discuss in Chapter-3. The integration of the CTS QDs with a photo-conduction structure based on SnS_2 nanoflakes results in a bandwidth enhancement in the structure discussed in Chapter-2 and Chapter-4 along with improved optical performance.

Finally, **Chapter-6** has been devoted to summarising the major findings of the thesis. At the end, the future scopes of the works related to the present thesis have been briefly outlined.